The Tibetan Plateau Space-based Tropospheric Aerosol Climatology: 2007–2020

Honglin Pan[1,2,3,4,5,6], Jianping Huang[1]*, Jiming Li[1], Zhongwei Huang[1], Minzhong Wang[2,3,4,5,6], Ali Mamtimin[2,3,4,5,6], Wen Huo[2,3,4,5,6], Fan Yang[2,3,4,5,6], Tian Zhou[1], Kanike Raghavendra Kumar[7]

[1]*Collaborative Innovation Center for Western Ecological Safety, College of Atmospheric Sciences, Lanzhou University, Lanzhou, 730000, China*

[2]*Institute of Desert Meteorology, China Meteorological Administration, Urumqi, 830002, China*

[3]*National Observation and Research Station of Desert Meteorology, Taklimakan Desert of Xinjiang, Urumqi, 830002, China*

[4]*Taklimakan Desert Meteorology Field Experiment Station of China Meteorological Administration, Urumqi, 830002, China*

[5]*Xinjiang Key Laboratory of Desert Meteorology and Sandstorm, Urumqi, 830002, China*

[6]*Key Laboratory of Tree-ring Physical and Chemical Research, China Meteorological Administration, Urumqi, 830002, China*

[7]*Department of Engineering Physics, College of Engineering, Koneru Lakshmaiah Education Foundation, Vaddeswaram, Guntur 522302, Andhra Pradesh, India*

Correspondence: Jianping Huang (hjp@lzu.edu.cn)

Abstract. A comprehensive and robust dataset of tropospheric aerosol properties is important for understanding the effects of aerosol-radiation feedback on the climate system and reducing the uncertainties of climate models. The third pole of Earth (Tibetan Plateau, TP) is highly challenging to obtain long-term in situ aerosol data due to its harsh environmental conditions. Here, we provide the more reliable new vertical aerosol index (AI) parameter from the spaceborne-based Lidar CALIOP onboard CALIPSO for daytime and nighttime to investigate the aerosol's climatology over the TP region during 2007-2020. The calculated vertical AI was derived from the aerosol extinction coefficient (EC), which was rigorously quality-checked and validation, and validated for passive satellite sensors (MODIS) and ground-based LIDAR measurements. Generally, our results demonstrated that there was agreement of the AI dataset with the CALIOP and ground-based LIDAR. Besides, the results showed that after removing the low-reliability aerosol target signal, the optimized data can obtain the aerosol characteristics with higher reliability. The data also reveals the patterns and concentrations of high-altitude vertical structure characteristics of the tropospheric aerosol over the TP. It will also help to update and make up the observational aerosol data in the TP. We encourage climate modelling groups to consider new analyses of the AI vertical patterns, comparing the more accurate datasets, with the potential to increase our understanding of the aerosol-cloud interaction (ACI) and aerosol-radiation interaction (ARI) and its climate effects. Data described in this work are available at https://data.tpdc.ac.cn/en/disallow/03fa38bc-25bd-46c5-b8ce-11b457f7d7fd

DOI:10.11888/Atmos.tpdc.300614. (Honglin Pan et al., 2023).

Keywords: Tibetan Plateau, CALIPSO, Aerosol index vertical structure, Tropospheric aerosols, Aerosol climatology.

1 Introduction

The three poles (i.e., the Arctic, the Antarctic and the Tibetan Plateau (TP)) have the highest mountains in the world and store more snow, ice and freshwater than any other place. The unique geographical location of the Antarctic, the Arctic, and the TP has unique ecological, climatic, and natural environmental changes. Also, the three locations have a crucial role in global and regional climate change. However, studies have found that these regions are susceptible to climate change. The differences in these regions may also affect key feedback loops for global climate change and the sustainability of human life. Unfortunately, our understanding of the three poles, particularly the relations between the regions, remains limited due to insufficient observation data. Currently, the collection of additional research data for these extreme environments is one of the major bottlenecks in facilitating comprehensive studies of these regions. Sufficient attention has been given to the polar regions and the TP in successive IPCC reports (IPCC, 2013 and 2021). The similarities between TP and the other two polar regions are their low temperatures, remote location, and large water storage capacity. On the other hand, TP has a more highly complex climate than the Arctic and the Antarctic (where ice is the primary medium) and its land surface (including forests, grasslands, bare soil, lakes and glaciers) is more diverse. These differences make the transport and accumulation of pollutants in the TP region different from the other two polar regions.

TP is known as the "Third Pole" because it has the third largest ice mass on Earth, after the Antarctic and the Arctic regions (Qiu, 2008). TP also called the "Asia Water Towers", provides fresh water to 40% of the world's population due to its vast water reserves such as glaciers, lakes and rivers (Immerzeel et al., 2010). Furthermore, TP is the "Roof of the World", which covers an area of ~2.5 million km^2 at an average altitude of about 4,000 m a.s.l. (above sea level) and includes all of Tibet and parts of Qinghai, Gansu, Yunnan, and Sichuan in southwestern China, as well as parts of India, Nepal, Bhutan, and Pakistan (Nieberding et al., 2020). To the north of the TP region is situated by the Taklamakan Desert (TD) (see Figure 1). This high altitude and specific

topographic area effectively serve as a heat source during the spring (MAM) and summer (JJA) months. This thermal structure helps the TP to function virtually as an "air pump", attracting warm and humid air from the lower latitude oceans by suction (Yanai et al., 1992; Wu and Zhang, 1998; Wu et al., 2007; Wu et al., 2012). Consequently, large-scale mountains play a crucial role in shaping regional and even global weather and climate through mechanical and thermodynamic effects and affect the global energy-water cycle (Xu et al., 2008; Molnar et al., 2010; Boos and Kuang, 2010; Wu et al., 2015). It is closely related to the survival of human beings in the world.

Climate projections are simulated responses of the climate system to future emission or concentration scenarios of greenhouse gases (GHGs) and aerosols and are generally calculated using climate models. The reasons for the gap between models and observations may also be due to inadequate solar, volcanic, and aerosol forcing used in the models, and in some modelling, may be due to an overestimation of the response to increasing GHG and other anthropogenic forcing (the latter includes the role of aerosols). The most significant uncertainties in predicting future climate change are related to uncertainties in the distribution and properties of aerosols and clouds, their interactions, and limitations in the representation of aerosols and clouds in global climate models (IPCC, 2021). The primary aerosol types over the TP is dust, which is primarily contributed from the Taklimakan Desert (Liu et al.,2008; Chen et al., 2013;2022; Xu et al., 2015). Previously some studies of aerosol-cloud interaction (ACI) and aerosol-radiation interaction (ARI) have been conducted (Liu et al., 2022). For example, the dust aerosols lifting over the TP reduce the radius of ice particles in the convective clouds and prolong the cloud lifetime through the indirect radiation effect, which can lead to the development of higher convective clouds. The dust-affected convective clouds move further eastward under the action of westerly winds and merge with local convective cloud masses, triggering heavy precipitation in the Yangtze River Basin and northern China downstream of the TP (Z. Liu et al., 2019; Y. Liu et al., 2019). However, the effect of aerosol on the atmospheric energy and water cycle remains uncertain, mainly due to the lack of long-term and accurate vertical aerosol optical properties dataset over the TP region. This can help better understand aerosol's impact

on the atmospheric heating rate and stabilization and the subsequent cloud-precipitation

process. Therefore, constructing a more long-term and reliable vertical dataset of

aerosol optical parameters can make up the observational facts for aerosol-related study

and provide a scientific basis for improving the global climate model simulation over

the TP.

Generally, the primary aerosol optical parameters (such as extinction coefficient

(EC), and aerosol optical depth (AOD)) acquisition method is in situ observations,

which have high precision. However, in situ observations are restricted by the

distribution of measurement stations over the TP. Hence, the resulting data lack spatial

continuity, making it difficult to meet the objectives of growing regional atmospheric

environmental studies (Chen et al.,2022; Goldberg et al.,2019; Giles et al., 2019).

Satellite remote sensing (active and passive) is an effective tool for collecting aerosol

optical information (including the vertical structure and spatial distribution) over a wide

range of spatial scales, significantly offsetting the deficiencies of in situ observations.

Satellite remote sensing can tackle difficulties connected to insufficient data and uneven

geographical distributions to a certain extent (Chen et al., 2022; Wei et al.,2021). While

for aerosol products observed from the Cloud-Aerosol Lidar and Infrared Pathfinder

Satellite Observations (CALIPSO), the presence of some low-reliability aerosol target

(LRAT) caused by cloud contamination, solar noise contamination, especially in the

daytime, and ground clutter among mostly aerosol observations skews the distribution

of the aerosol EC towards larger values, at least some of which may be identified as

aerosols and retained in the analysis, makes the presence of some low confidence

aerosol targets bias the distribution of aerosol extinction in most aerosol observations.

The distribution of the aerosol EC will show greater biased values (Thomason and

Vernier, 2013; Kovilakam et al., 2020; Pan et al., 2020; Kahn et al., 2010), and then will

further enhance the aerosol index (AI) value due to the influence of radiation transfer

interaction between clouds and the absorption layer, which will not truly reflect the

differences in aerosol physical properties (Guan et al., 2008; Liu et al., 2019; Kim et

al.,2018). Hence, gaining high confidence in EC helps us analyze aerosol optical

properties and leads to numerous pertinent uses of EC data, which is essential for

148   accurately characterizing the upper range of aerosol ECs that occur on the TP.

149   The present study provides a dataset of monthly averaged vertical structure

150   characteristics of tropospheric high confidence aerosol optical properties including EC,

151   AOD, Angstrom exponent (AE), and aerosol index (AI) in the daytime and nighttime

152   over the TP and surrounding areas. The data for the above-mentioned optical properties

153   were retrieved based on the space-borne Lidar CALIOP (Cloud-Aerosol Lidar with

154   Orthogonal Polarization) on board the CALIPSO satellite for the period 2007-2020.

155   The main objective of this study is to calculate new and high-confidence aerosol optical

156   parameters of AI in the vertical distribution, by the strict quality control and validation

157   for passive remote sensing satellite sensor (MODIS) and active remote sensing ground-

158   based LIDAR. AI is dependent on aerosol concentration, optical properties and altitude

159   of the aerosol layer. Also, AI is particularly sensitive to high-altitude aerosols, which is

160   used to indicate small particles (those that act as cloud condensation nuclei) with a high

161   weight (Guan et al., 2010; Buchard et al., 2015; Liu et al., 2019; Nakajima et al., 2001).

162   The comprehensive data set of aerosol optical properties utilized in the study is of

163   substantial importance for understanding the impact of aerosol on the ecosystem and

164   reducing the uncertainties of climate models.

165   The data set used in this study is more effective to characterize the vertical

166   structure of aerosols while following standardized quality control methods to obtain

167   higher confidence in the aerosol vertical structural properties covariate data sets and

168   allow for comparison and application to the study of climate models and other

169   atmospheric science related problems between our records and other public different

170   data sets. To ensure meaningful confidence estimates, it is necessary to apply carefully

171   the following correction procedures and analytical validation for the constructed

172   aerosol covariates over the TP. The main steps to construct the dataset are grouped as

173   follows: (1) Removing the low-confidence aerosol EC at 532 nm and 1064 nm caused

174   by the misclassification of cloud and other interferences (e.g., surface clutter,

175   hygroscopicity etc.). Based on this, an interquartile range (IQR) method (see section

176   2.2) is utilized to discard the low confidence targets, and further obtain the monthly

177   averaged aerosol EC for day and nighttimes with higher confidence; (2) the pseudo-

Ångström exponent (hereafter AE) is calculated using the aerosol EC at 532 nm and 1064 nm with higher confidence; (3) obtaining vertical AI by the product of the AOD (the vertical layers integral of EC) and AE. (4) Validation for the constructed AI with MODIS and in situ LIDAR measurements using the standardized frequency distributions.

2 The construction of the data set

2.1 Study area

Figure 1 depicts the geopotential height of the TP and its surrounding areas (27-42°N,75-102°E, about 4,000 m a.s.l.), and a schematic diagram of CALIPSO satellite ground track over the TP in different months. The role of the "heat-driving air pump" of the TP provides abundant water vapor for the formation of clouds (Luo et al., 1984; Liou et al.,1986). Furthermore, the TP environment is greatly affected by natural and anthropogenic aerosols from the surrounding regions (Chen et al., 2013; Bucci et al.,2014; Xu et al.,2015). The strong convection generated by the TP will promote aerosols' vertical transport and increase aerosols' content in the troposphere and stratosphere (Vernier et al., 2015; Liu et al., 2022). Aerosols also serve as cloud condensation nuclei (CCN) or ice nuclei (IN), modifying cloud structure properties and precipitation (Twomey et al.,1977). Hence, the TP has been called as the pumping pump of water vapor, the cloud incubator, and the sand dust transfer station. By delivering water vapor, clouds, and dust, it regulates extreme weather and climate in the downstream and surrounding areas. It can be seen that the TP plays a crucial role in the impact and regulation of global and regional climate or environments (Luo et al.,1984; Rossow et al., 1999; Wan et al.,2017; Liu et al., 2022).
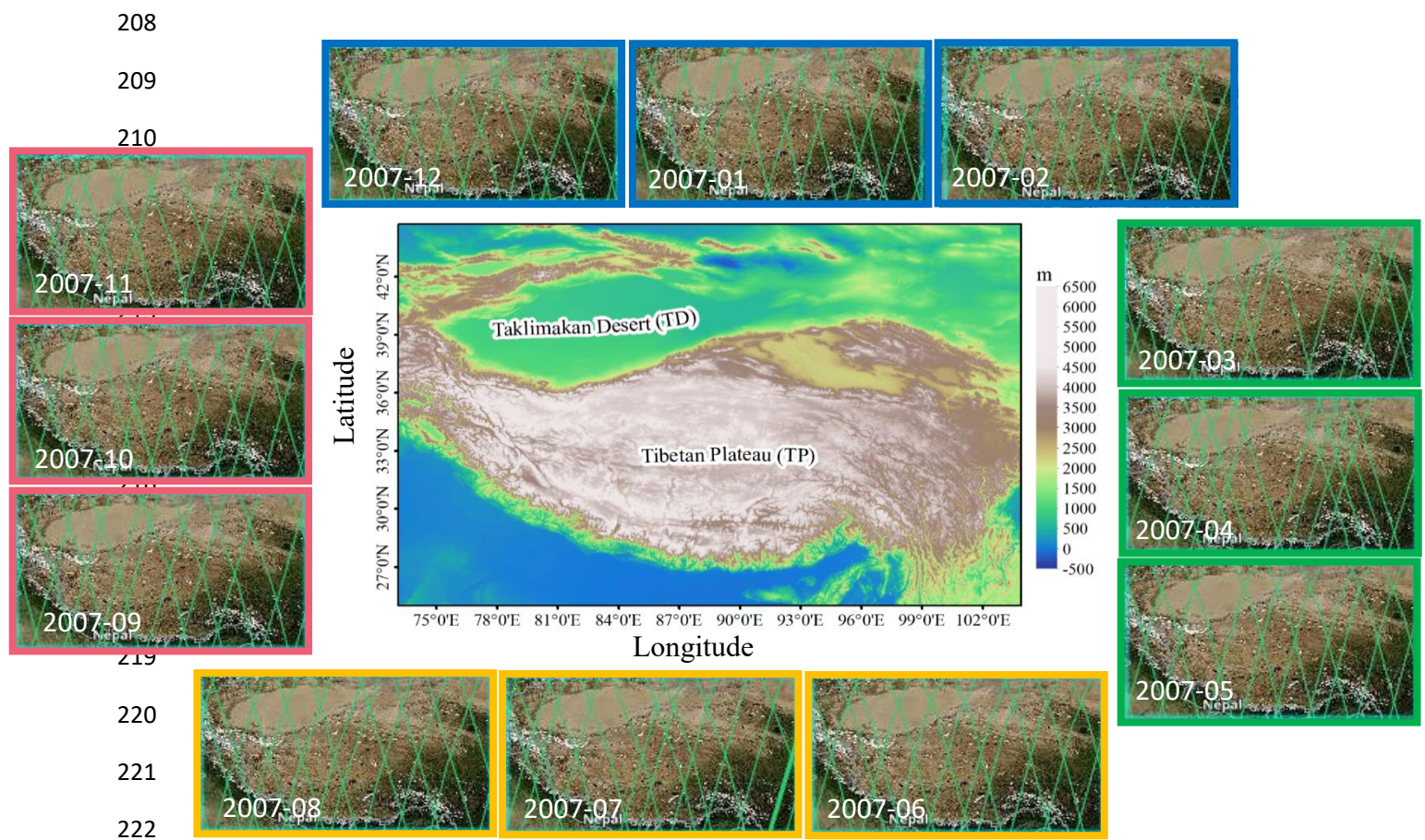
208

209

210

Figure. 1 The geopotential height of the TP and its surrounding areas (27-42°N,75-102°E). The schematic diagram of the transit of the CALIPSO satellite orbits over the TP in all months of 2007 (with 2007 as an example). The seasons have been classified as March-May is spring, June-August is summer, September-November is autumn, and December-February is winter).

2.2 CALIOP data and low-reliability aerosol target (LRAT) clearing method

The CALIOP, onboard the CALIPSO satellite was launched by the NASA on 28 April 2006, is the nadir-pointing dual-wavelength polarization Lidar, which can provide global and continuous information on the vertical distribution of aerosols and clouds at 532 nm and 1064 nm for daytime and nighttime (Winker e t al., 2007 and 2009). The CALIPSO-CALIOP (version 4.20) level-2 aerosol profile product is selected in this study, with vertical and horizontal resolutions of 60 m and 5 km, respectively. The used parameter includes Extinction_Coefficient_532 and Extinction_Coefficient_1064 between daytime and nighttime observations from 2007 to 2020. It should be noted that the CALIOP data uses as few instruments as necessary to complete the monthly aerosol climatology. We make this decision to limit the impact of differences between

238   instruments due to measurement techniques and wavelength range as well as assess the

239   general quality of the instrument's data set.

240   The presence of some low-reliability aerosol target (LRAT) caused by cloud

241   contamination, solar noise contamination, especially in the daytime, and ground clutter

242   among mostly aerosol observations skews the distribution of the aerosol EC toward

243   larger values (Thomason and Vernier, 2013). Consequently, to eliminate the LRAT, a

244   statistical approach to identify LRAT and extreme outliers is utilized based on the

245   interquartile range (IQR). IQR is a more conservative measure of the spread of

246   distribution than standard deviation (Iglewicz and Hoaglin, 1993). Note that this

247   technique is based on median statistics rather than the mean due to the skewed

248   distribution of EC. In our implementation, we used daily data at each altitude (0.06 km)

249   and latitude (0.05°) bin from 2007-2020 to determine frequency distribution of EC for

250   different months. Besides, we used the lower quartile (Q1) and upper quartile (Q3) of

251   the underlying distribution to find IQR, defined as Q3-Q1, a good measure of the spread

252   in the data relative to the median. Here, an extreme outlier is defined as Q3 + (3.5×IQR),

253   and a more upper outlier (Q3+(1.5×IQR)) is used for comparison (Iglewicz and Hoaglin,

254   1993). Meanwhile, the extreme outlier threshold is used to clear LRAT-affected

255   observations from the data set, which is better and more effective at identifying outliers

256   in the density distribution (Kovilakam et al., 2020).

257   **2.3 AI Data Processing**

258   According to the method described in section 2.2, the aerosol EC (observed at 532

259   nm and 1064 nm for daytime and nighttime) with higher reliability over the TP is

260   obtained. The monthly mean Ångström exponent (hereafter "pseudo-Ångström

261   exponent (AE)") for daytime and nighttime is derived to establish the 14-year aerosol

262   climatology (2007-2020) based on equation (1). The AE model for EC which is

263   wavelength dependence at 532 and 1064 nm is given by Kovilakam et al. (2020):

$$EC_{-532[m,i,j]} = EC_{-1064[m,i,j]} \left(\frac{\lambda_{532}}{\lambda_{1064}} \right)^{AE[m,i,j]}$$

264   (1)

265   where $EC_{-532[m,i,j]}$ and $EC_{-1064[m,i,j]}$ are extinction coefficients at 532 nm and 1064 nm,

266 respectively; AE [m, i, j] is the pseudo-Ångström exponent (Rieger et al.,2015;2019);

267 and the indices [m, i, j] represent the month, latitude, and altitude respectively.

268 $(\lambda_{532}/\lambda_{1064})$ represents the ratio of wavelengths at 532 nm and 1064 nm. The AE is

269 gridded to 0.05 ° latitude and 0.06 km altitude resolution. Further, the vertical

270 distribution of AI is calculated according to equation (2). AI has been developed by

271 Nakajima et al. (2001) and Liu et al. (2019) with the equation given below:

272 $$AI_{[m,i,j]} = AOD_{[m,i,j]} \times AE_{[m,i,j]} \tag{2}$$

273 Where $AI_{[m,i,j]}$ and $AOD_{[m,i,j]}$ are aerosol index and aerosol optical depth, respectively;

274 $AE_{[m, i, j]}$ is the pseudo-Ångström exponent; and [m, i, j] represent the month, latitude,

275 and altitude respectively. Note that to match the AE, AOD is also transformed into the

276 vertical distribution (not the column parameter). As we focus on the characteristics of

277 aerosols in the troposphere over the TP, we took samples from the surface at an altitude

278 of 12 km with a vertical resolution of 0.06 km. We integrated the EC of each two layers

279 to obtain an AOD, which corresponds to the average of the AE values of each two layers.

280 This achieves spatial matching between AOD and AE at the vertical heights. In the later

281 stage, when using the AI obtained from MODIS for comparative testing, we used the

282 PDF (probability density function) and average values of AI for characterization

283 displayed to facilitate comparison due to the differences in horizontal and vertical space.

284 The data in this manuscript are all based on the vertical structural distribution of

285 altitude-latitude with vertical and horizontal resolutions of 60 m and 0.05 ° ,

286 respectively. The monthly mean climatology of AI is retrieved from the CALIOP and

287 computed in altitude and latitude at 532 nm and 1064 nm for the daytime and nighttime

288 data sets.

289 **2.4 Aqua-MODIS satellite data**

290 Like the CALIPSO, Aqua is part of the A-Train constellation of satellites.

291 Therefore, the MODIS (Moderate-resolution Imaging Spectroradiometer) onboard

292 Aqua can achieve near-simultaneous observations of clouds and aerosols with

293 CALIPSO-CALIOP (less than two minutes) (Winker et al., 2007; Hu et al., 2010). The

294 Aqua satellite was successfully launched on May 4th, 2002. Aqua is the afternoon star,

passing through the equator from south to north at around 13:30 local time. The observation data of 36 wavebands were obtained, with a maximum spatial resolution of 250 m and a scanning width of 2330 km. MODIS is a passive imaging spectroradiometer, and there are a total of 490 detectors distributed in 36 spectral bands, with full spectral coverage ranging from 0.4 microns (visible light) to 14.4 microns (thermal infrared). In this study, Level 3 data (MYD08_M3) on a 1°×1° (longitude × latitude) gridded box is utilized. As shown in Table 1, MODIS can provide AOD and AE products at 550 nm wavelength. It is worth mentioning that we chose this data because MODIS data is widely used and has certain reliability in aerosol research. The parameters of AE and AOD from MODIS are also used to calculate the AI, which is applied to evaluate the monthly mean climatology of AI from CALIOP over TP (see Table 1).

Table 1 Comparison between MODIS and CALIOP existing data products (√ represents the existing data products of the satellite, NAN indicates non-existent, × represents non-existent data product parameters that need further calculation in this study).

Detector/Satellite	Wavelength	Extinction Coefficient (EC)	Aerosol Optical Depth (AOD)	Angstrom Exponent (AE)	Aerosol Index (AI)
CALIOP/CALIPSO (active)	532nm&1064nm	√	√	×	×
MODIS/Aqua (passive)	550nm	NAN	√	√	×

2.5 Ground-based LIDAR data

Besides, we used the ground-based LIDAR (Light Detection and Ranging) (38.967 ° N, 83.65 ° E, 1099.3m) detection data from the hinterland of the Taklimakan Desert (TD) to verify the validity and accuracy of the low confidence aerosol removal method and the AI calculated by CALIOP detection data. Multi-band Raman polarization LIDAR (hereafter LIDAR) is mainly used for the detection of dust, aerosols, and cloud particles in the atmosphere, which detection belongs to "Belt and

Road" Lidar Network from Lanzhou University, China (http://ciwes.lzu.edu.cn/), has an advantage with calibrate or validate Satellite observation (see Figure 2). The primary technical specifications of LIDAR are mentioned in Table 2. For the performance of LIDAR and the data inversion of aerosol-related optical parameters, the authors advise the readers to refer to the research work of Zhang et al. (2022, 2023).
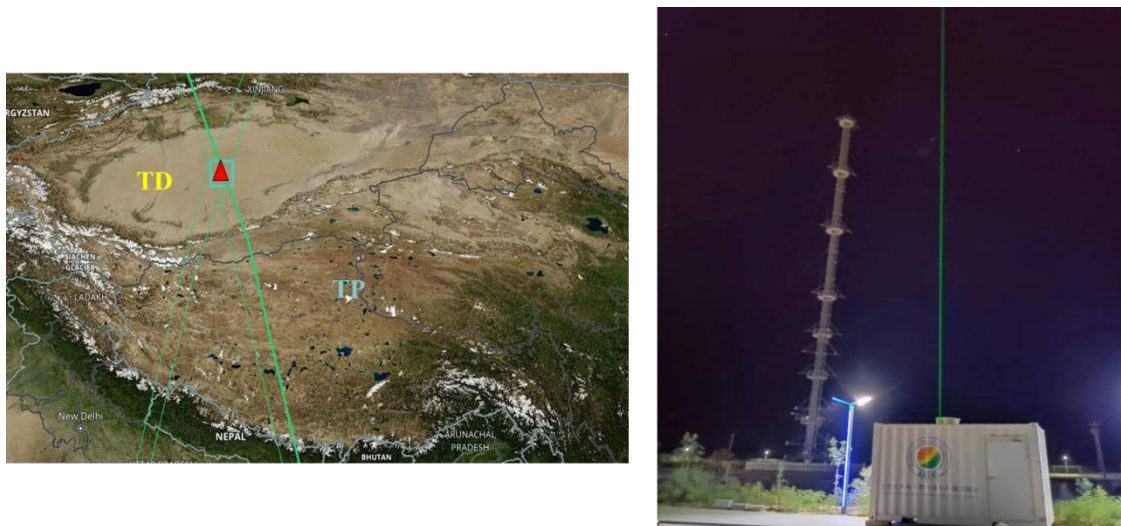
Figure 2. CALIPSO satellite orbit passes through the central area of the Taklimakan Desert hinterland-left (the red triangle represents the observation coordinates of the ground-based LIDAR - right (38.967 ° N, 83.65 ° E, 1099.3m), TD - Taklimakan Desert, TP - Qinghai Tibet Plateau) (pictures from NASA'S Earth data (left) and photography(right)).

Table 2. Basic technical specifications of LIDAR from the hinterland of the Taklimakan Desert (TD).

Detection range	Spatial resolution	Laser wavelength	Laser energy	Pulse frequency
0~20km	7.5m	532nm/1064nm	100mJ	20Hz

In this study, based on the Level_2 aerosol profile data product (extinction coefficient, EC) for daytime and nighttime detected by CALIOP from 2007 to 2020, the low-reliability aerosol target (LRAT) is screened and eliminated. The aerosol characteristic data set with higher reliability over the TP is constructed, and the data set is verified and compared with MODIS and ground-based LIDAR to test its effectiveness and accuracy. Thus, the vertical structure of aerosol properties and its climatology with higher reliability over the TP can be obtained, providing adequate observation facts and a basis for the TP. All steps were implemented and processed as

338   follows shown in Figure 3.
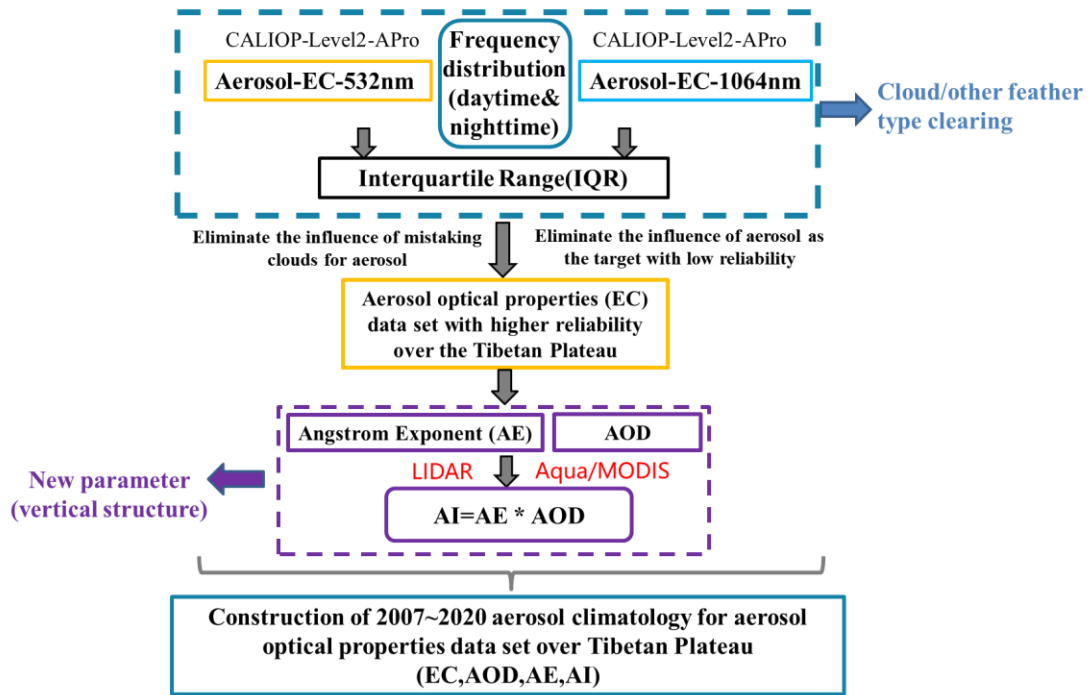
Figure 3. Flow chart of the construction and calculation process of aerosol optical characteristics data set over the TP.

3 Results and discussion

3.1 Screening and elimination of Low-Reliability Aerosol Target (LRAT)

In this section, we screened and eliminated LRAT for tropospheric aerosol EC from the CALIOP over the TP, based on the statistical method (see Section 2.2). Figures 4 and 5 show the monthly frequency distribution of EC detected by the CALIPSO-CALIOP at 532 nm and 1064 nm in the daytime during 2007-2020. While Figures 6 and 7 are the same, but for the nighttime. It is observed that all Figures 4-7 demonstrated the non-normal distribution of aerosol EC for the daytime and nighttime. It is found that the upper outlier appeared to remove many enhanced aerosol measurements when more sand and dust events occurred in the surrounding areas and rose to the TP in spring and summer. In contrast, the extreme outlier was effectively identified in the frequency distribution. Therefore, the extreme outlier threshold is used to clear LRAT observations from the CALIOP data set which is necessary.

After the screening and elimination of LRAT, the monthly aerosol climatology

356   data and extreme outliers are compared for the years 2007-2020. We found that during

357   the daytime for 532 nm and 1064 nm, the aerosol EC over the TP is mainly concentrated

358   between 0 and 0.2. The extreme outliers in July and August are more significant than

359   those in other months, related to the rising motion of the TP as a heat source in summer

360   to trigger convection. This results in more ice clouds in the upper air, thus increasing

361   the probability of misclassification of the cirrus anvil as an aerosol (Carrió et al., 2007;

362   Kojima et al., 2004; Seifert et al., 2007). Also, the aerosol data points (samples) are the

363   largest in May and the smallest in November over TP. Obviously, the aerosol samples

364   are more in the spring and summer seasons than in autumn and winter. This is related

365   to the frequent sand and dust activities in the spring and summer seasons around the TP

366   (such as the Taklimakan Desert) and anthropogenic pollution (Y. Liu et al., 2019, as

367   mentioned earlier).

368   Similarly, during the nighttime for 532 nm and 1064 nm, the aerosol EC over the

369   TP is mainly concentrated between 0 and 0.1, and the extreme outliers in July and

370   August are more significant than those in other months. However, the aerosol EC

371   observed in the nighttime is smaller than the daytime data set. The primary

372   consideration is that the daytime solar noise is considerable and the signal-to-noise ratio

373   of LIDAR observation is low, which further increases the probability that the aerosol

374   EC presents a skewed distribution; It can be seen that the elimination of LRAT from

375   daytime data is more conducive to improving the accuracy of data. Meanwhile, the

376   aerosol data points are the largest in April and the smallest in December over the TP. It

377   can be seen that in April (spring), more aerosol samples were lifted and transported to

378   the TP. Numerous observations have shown elevated dust plumes lofted into the free

379   troposphere during spring, and air parcels between 4 km and 7 km mainly originate

380   from the TD (Huang et al.,2008; Sasano,1996; Liu et al.,2008; Zhou et al.,2002;

381   Matsuki et al., 2003). It is the same as the daytime with spring and summer being more

382   than autumn and winter, while there is one order of magnitude larger than the daytime

383   data. It is not difficult to see that the CALIOP is less sensitive during daytime than

384   nighttime due to signal-noise-ratio reduction by solar background illumination, which

385   leads to weakly scattering layers can be detected during nighttime while missed during

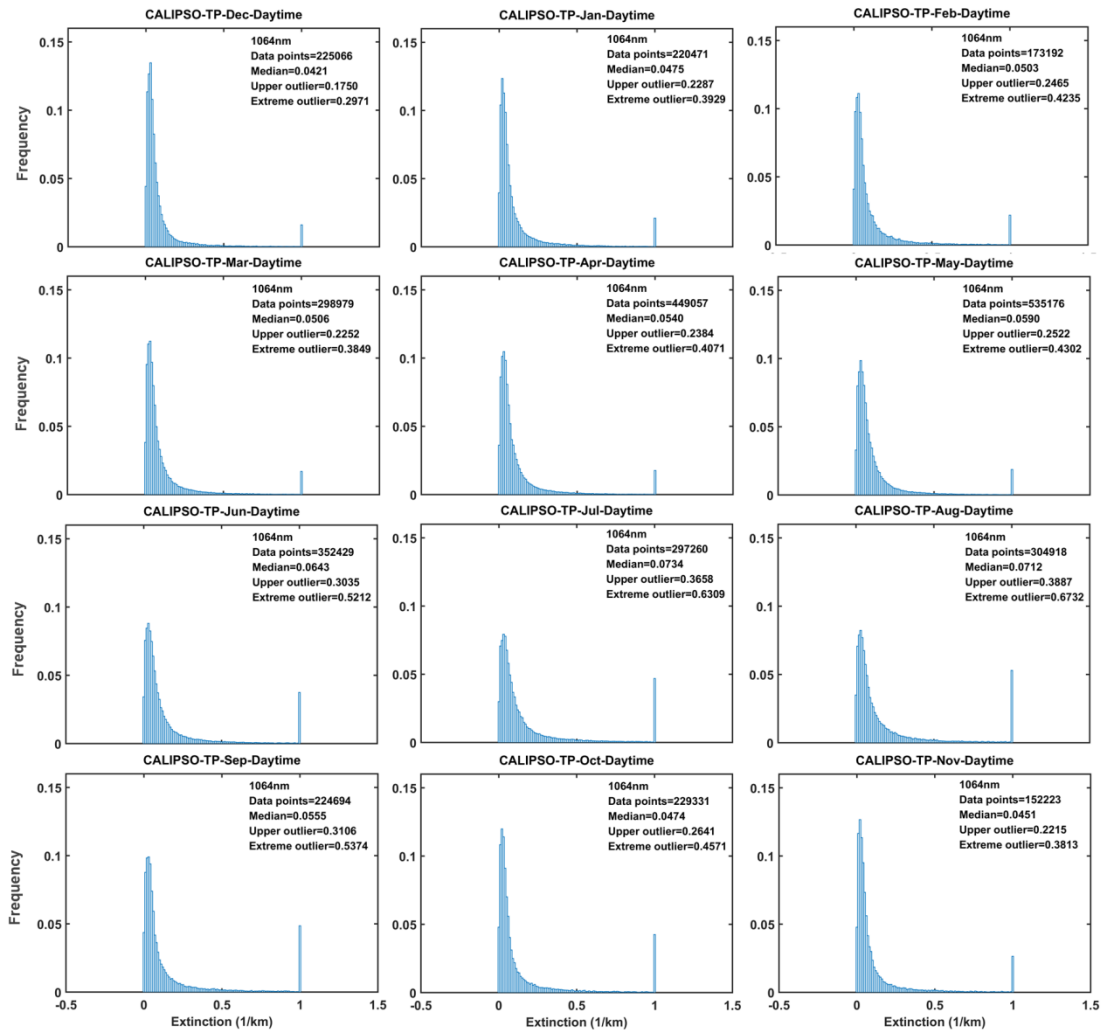386   daytime (Huang et al., 2013; Liu et al.,2009).

387
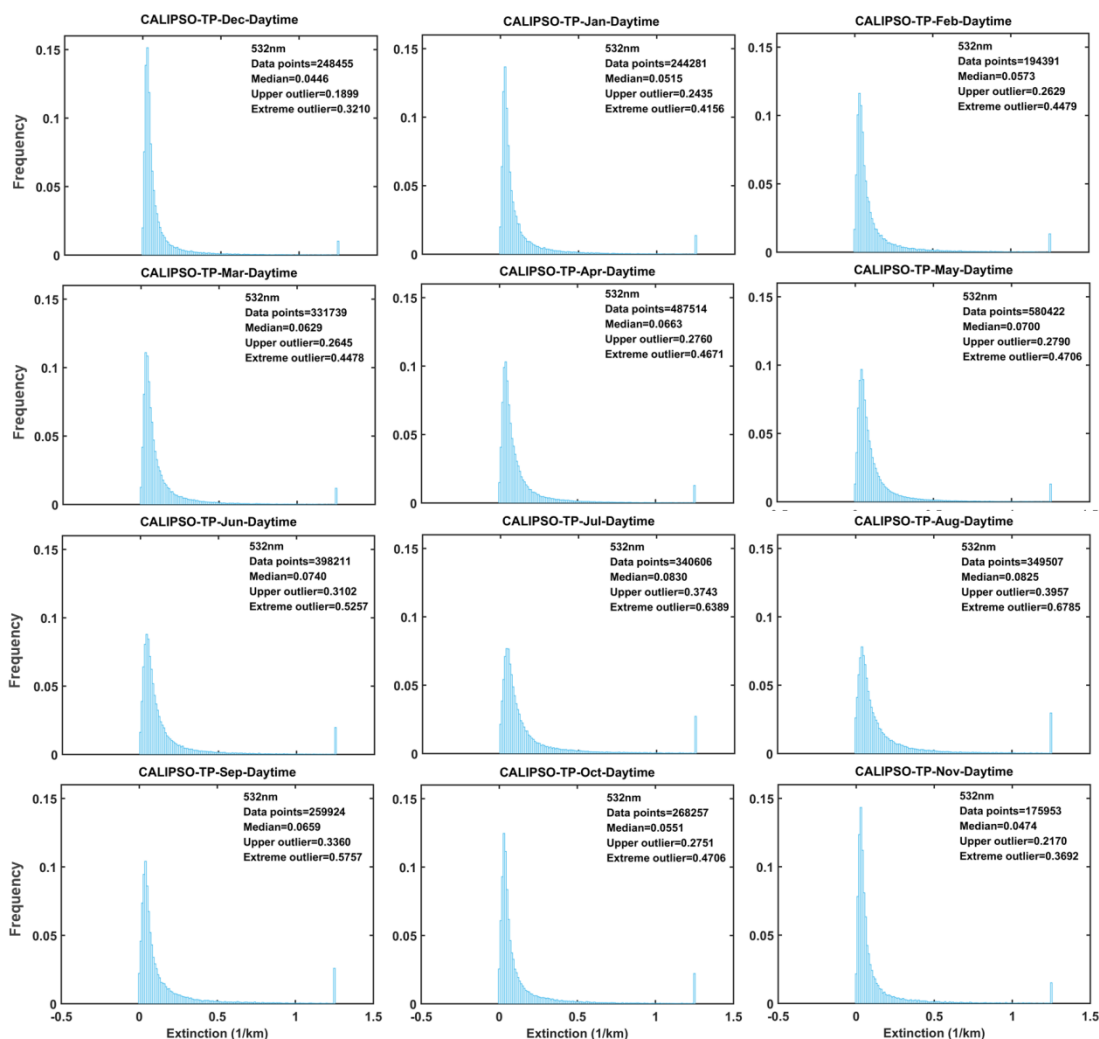
388
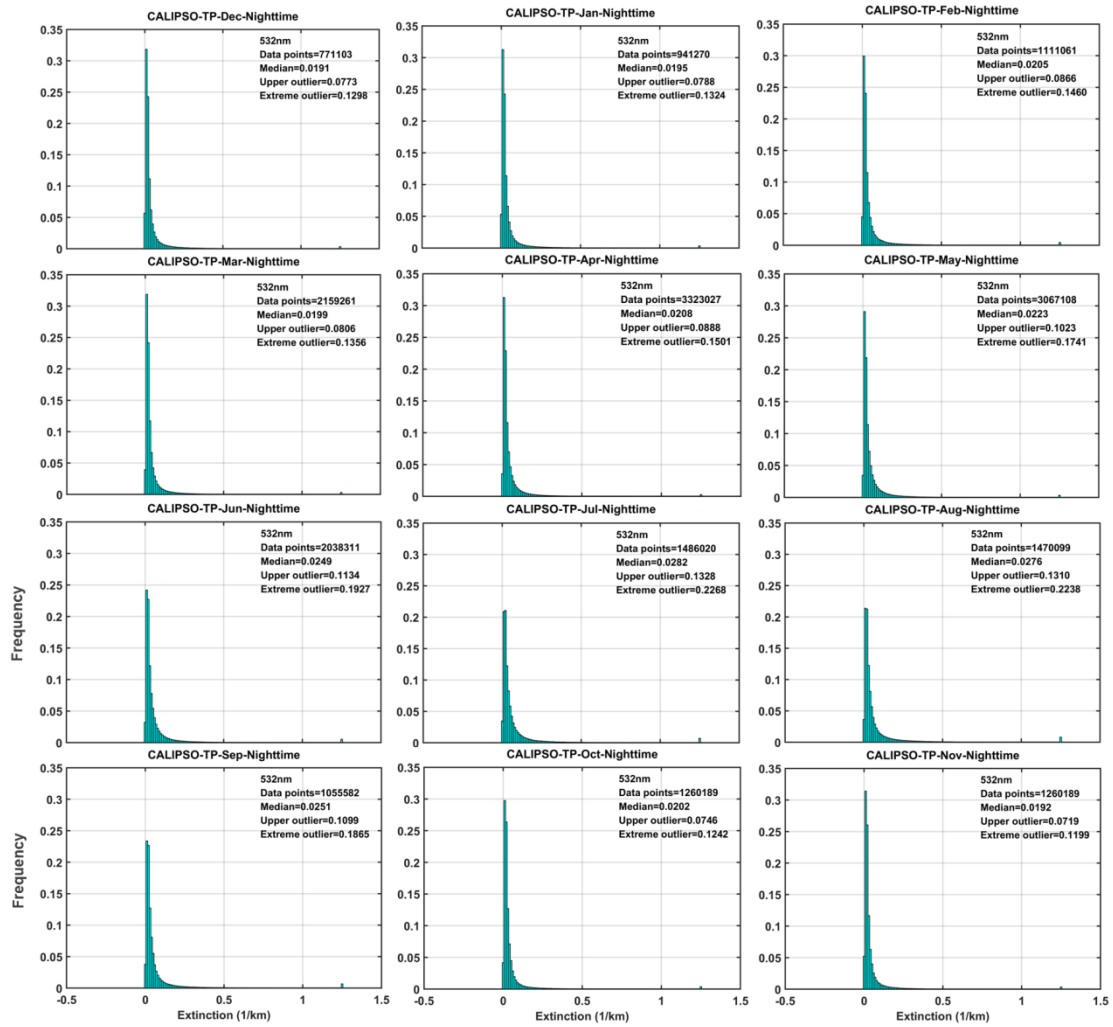
389   Figure 4. Monthly frequency distribution of aerosol extinction coefficient at 532 nm over the Tibet

390   Plateau (TP) in the daytime during 2007-2020 from January to December (Panels in the first, second,

391   third, and fourth rows corresponds to Winter (December-February), Spring (March-May), Summer

392   (June-August), and Autumn (September-November). The frequency distribution is the number of

393   events normalized to the maximum value. The Upper outlier, extreme outlier and median are also

394   shown in all panels.

395

396

397

Figure 5. The same as in Figure 4, but for 1064nm.

Figure 6. Monthly frequency distribution of aerosol extinction coefficient at 532 nm over the Tibet Plateau (TP) in the nighttime during 2007-2020 from January to December (Panels in the first, second, third, and fourth rows corresponds to Winter (December-February), Spring (March-May), Summer (June-August), and Autumn (September-November). The frequency distribution is the number of events normalized to the maximum value. The Upper outlier, extreme outlier and median are also shown in all panels.
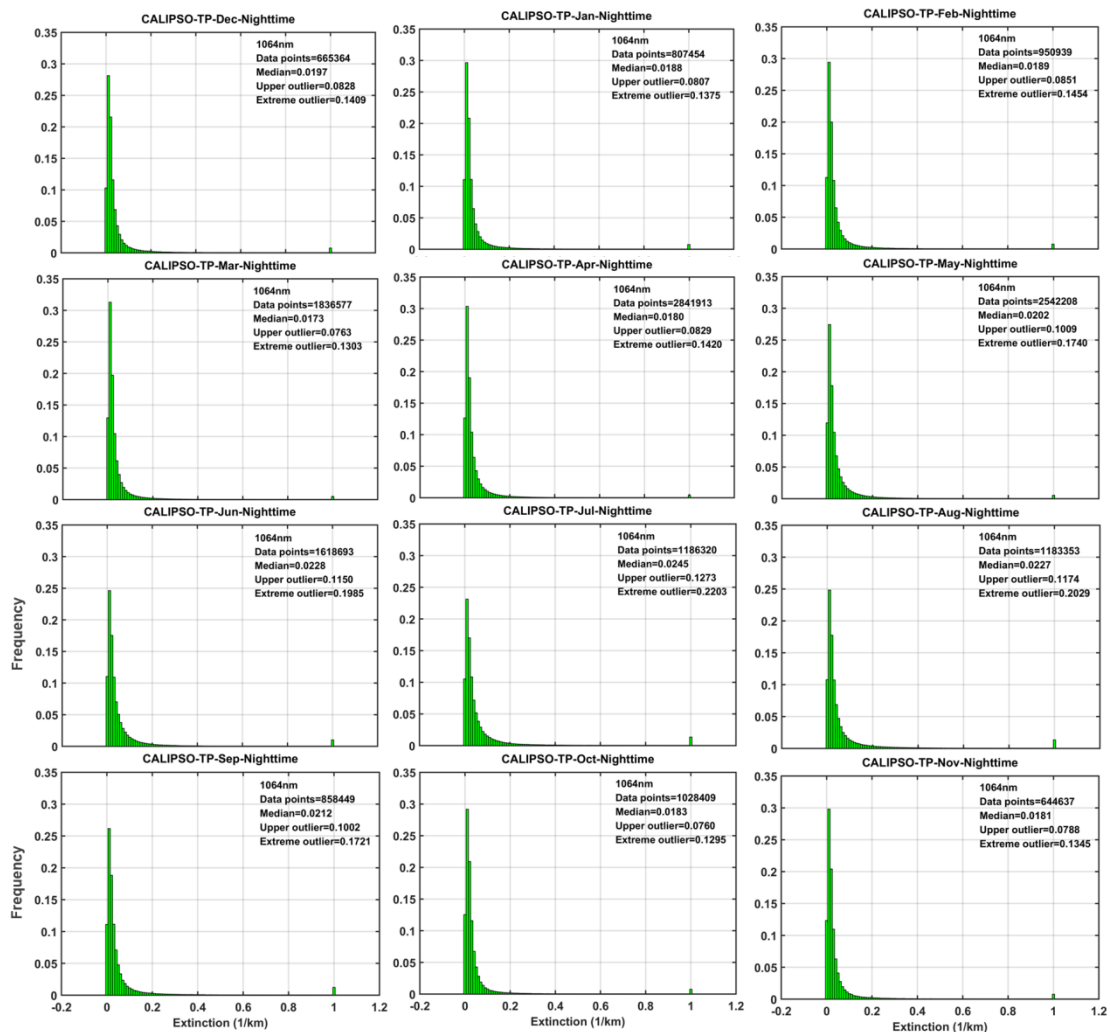
Figure 7. The same as in Figure 6, but for 1064 nm.

3.2 Constructing vertical aerosol index (AI) for daytime and nighttime

Figures 8 and 9 show daytime altitude-latitude plots of the monthly climatology of aerosol EC at 532 nm and 1064 nm before and after the screen, respectively. The monthly mean climatology of the pseudo-Ångström exponent (AE) and Aerosol Index (AI) vertical structure is then computed as shown in Figure 10. We choose typical months of January, April, July, and October to represent the respective seasons of winter, spring, summer, and autumn. Figures 8 and 9 show that extreme outliers in the troposphere over the TP have been eliminated, especially in the lower layer, where more obvious LRAT have been identified and eliminated. In the upper layer (more than 7 km), especially in April and July (i.e., spring and summer), weak cirrus signs may exist in the original aerosol signals and be eliminated. Compared with other seasons, the aerosol on the TP is widely and uniformly distributed in the troposphere in April, indicating

18

that in general, more aerosol loads are lifted over the TP in April. In Figure 10, we compute values between 0 and -1 for much of the troposphere and occasionally are between 0 and 2 in the middle troposphere (less than 8 km), which has similar results or pattern in Kovilakam's study (Kovilakam et al., 2020). Note that the derived value for pseudo-AE is without the physical meaning, and it is simply a means to combine AOD to obtain AI of vertical structure. Using this climatology of pseudo-AE values, we can effectively convert any month of AI data to 532 nm and 1064 nm because the fixed AE is not necessarily applicable to retrieving aerosol extinction in all months. Relevant research points out that the accuracy has been improved using the corresponding AE of each month to correct the satellite data (Kovilakam et al., 2020).

Figure 10 also demonstrates the distribution characteristics of AI values at 532 nm and 1064 nm in different seasons over the TP in the daytime. In all seasons, AI is mainly distributed between -0.04 and 0.04. Still, the proportion between 0 and -0.02 is the largest. Here, we have a broad understanding of traditional AI. AI is a way to measure how backscattered ultraviolet (UV) radiation from an atmosphere containing aerosols differs from that of a pure molecular atmosphere (Guan et al., 2010). AI is especially sensitive to the presence of UV-absorbing aerosols such as smoke, mineral dust, and volcanic ash. AI, positively suggests the existence of absorbent aerosols (dust, black carbon, etc.); A small or negative AI suggests the presence of non-absorbable aerosols or clouds) (Hu et al.,2020; Guan et al., 2010; Hammer et al., 2018). AI varies with aerosol layer height, optical depth, and single scattering albedo (Torres et al., 1998;2007; Hsu et al.,2004; Jeong and Hsu, 2008). However, the significance of obtaining vertical structure AI in our research content is different from that of traditional AI representation. The AI obtained from our research work cannot effectively characterize the absorption and non-absorption of its aerosols, as the results obtained are in the non-ultraviolet band range. However, the aerosol concentration represented by the vertical structure AI is not possessed by column AOD. Compared to the aerosol column concentration AOD information, as AOD is an integral result of the entire layer height, it will to some extent lose some of the true changes in the vertical height of aerosols. The significance of our work is that the AI with higher reliability obtained here can more effectively obtain

461   aerosol concentration information at vertical height. In the four seasons, the distribution

462   of aerosols in the north is broder than that in the south; In spring, the rise height of

463   aerosol is higher and the vertical distribution range is more comprehensive. The

464   elevation in summer is lower than that in the other three seasons, but the aerosol species

465   are more abundant because there are many ranges of AE values.

466
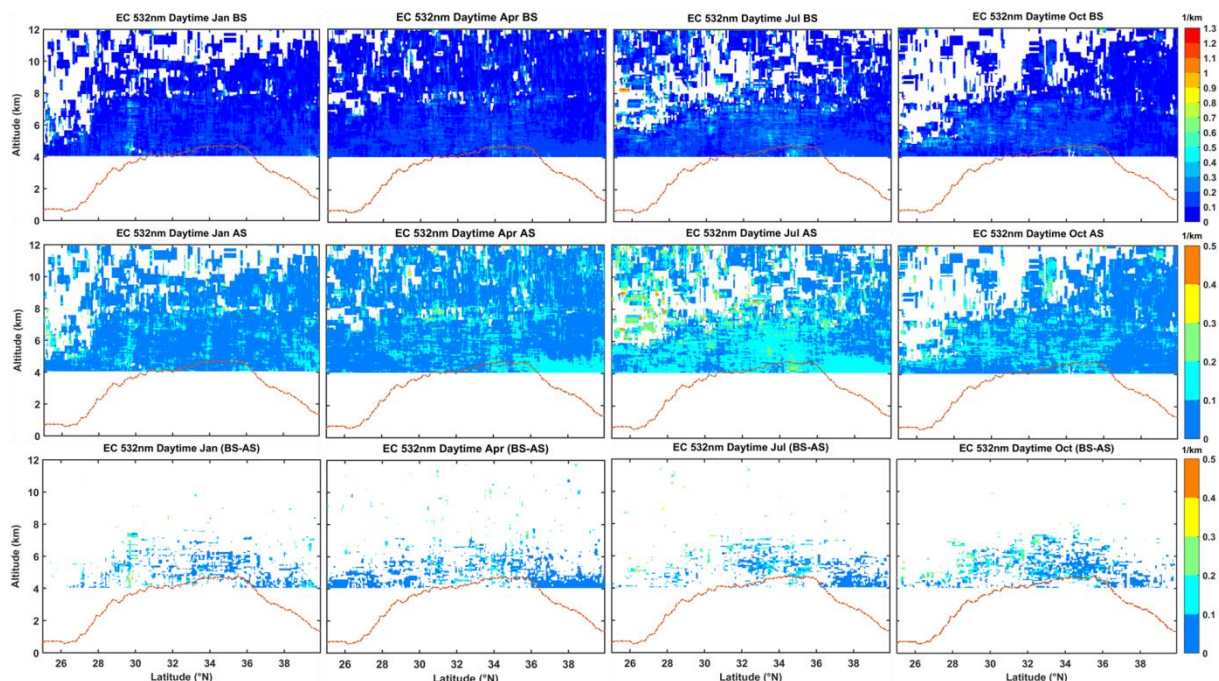
467

468   Figure 8. The monthly average comparison and difference of aerosol extinction coefficient at 532

469   nm before and after elimination of low-reliability aerosol target (LRAT) over Tibet Plateau (TP) for

470   daytime during 2007-2020. The reddish-brown dotted line denotes the surface. (BS: Before

471   Screened, first line; AS: After Screened, second line; (BS-AS) means Before Screened minus After

472   Screened, representing spatial lattice with screening and elimination, third line)

473
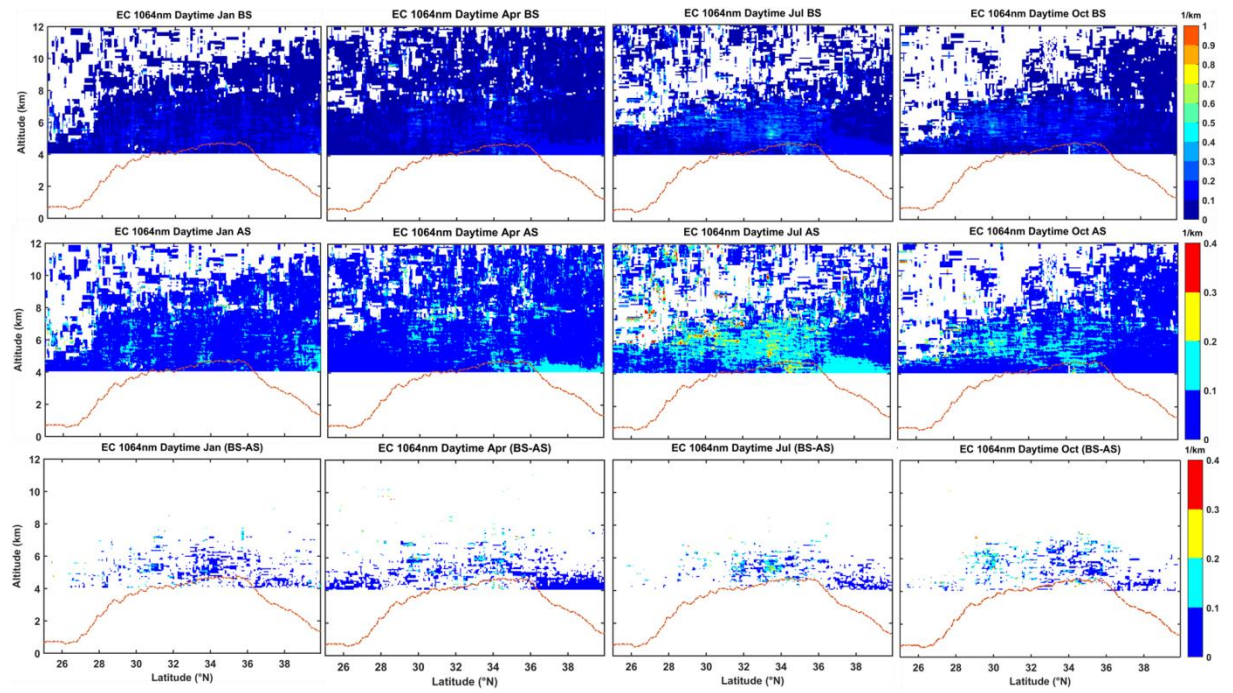
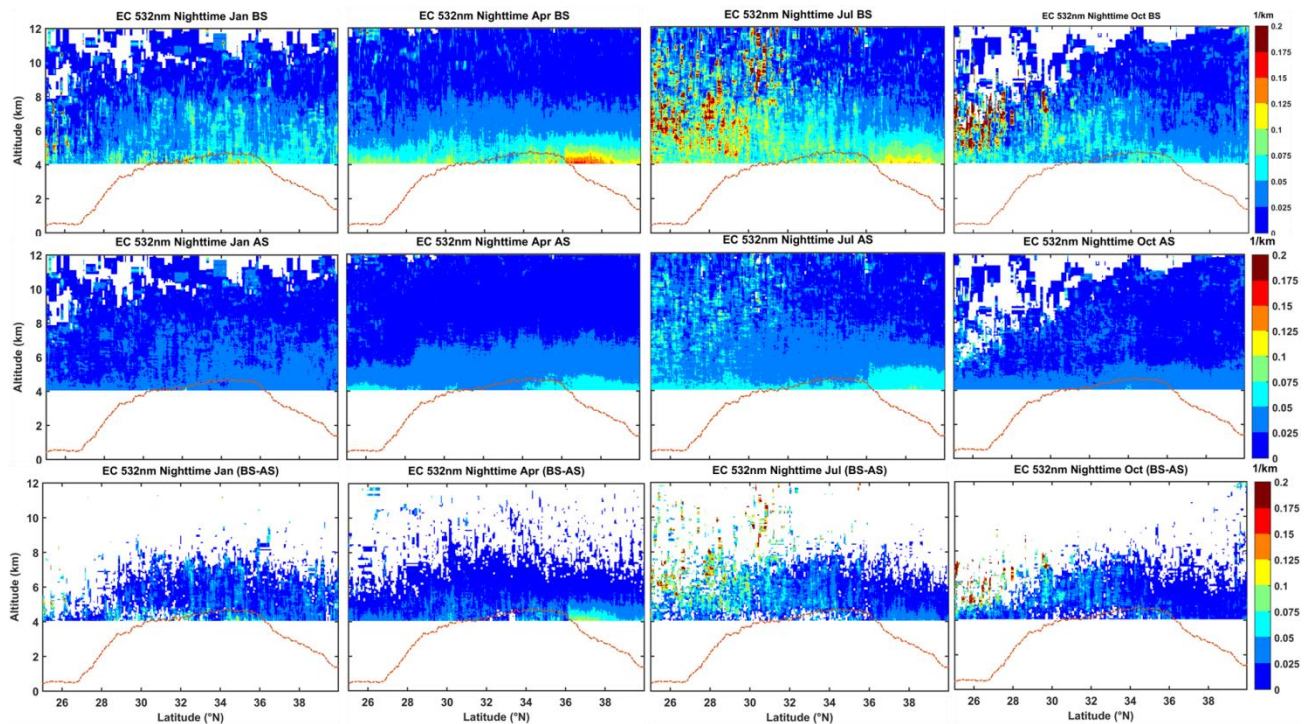Figure 9. The same as in Figure 8, but for aerosol EC at 1064 nm for the daytime.
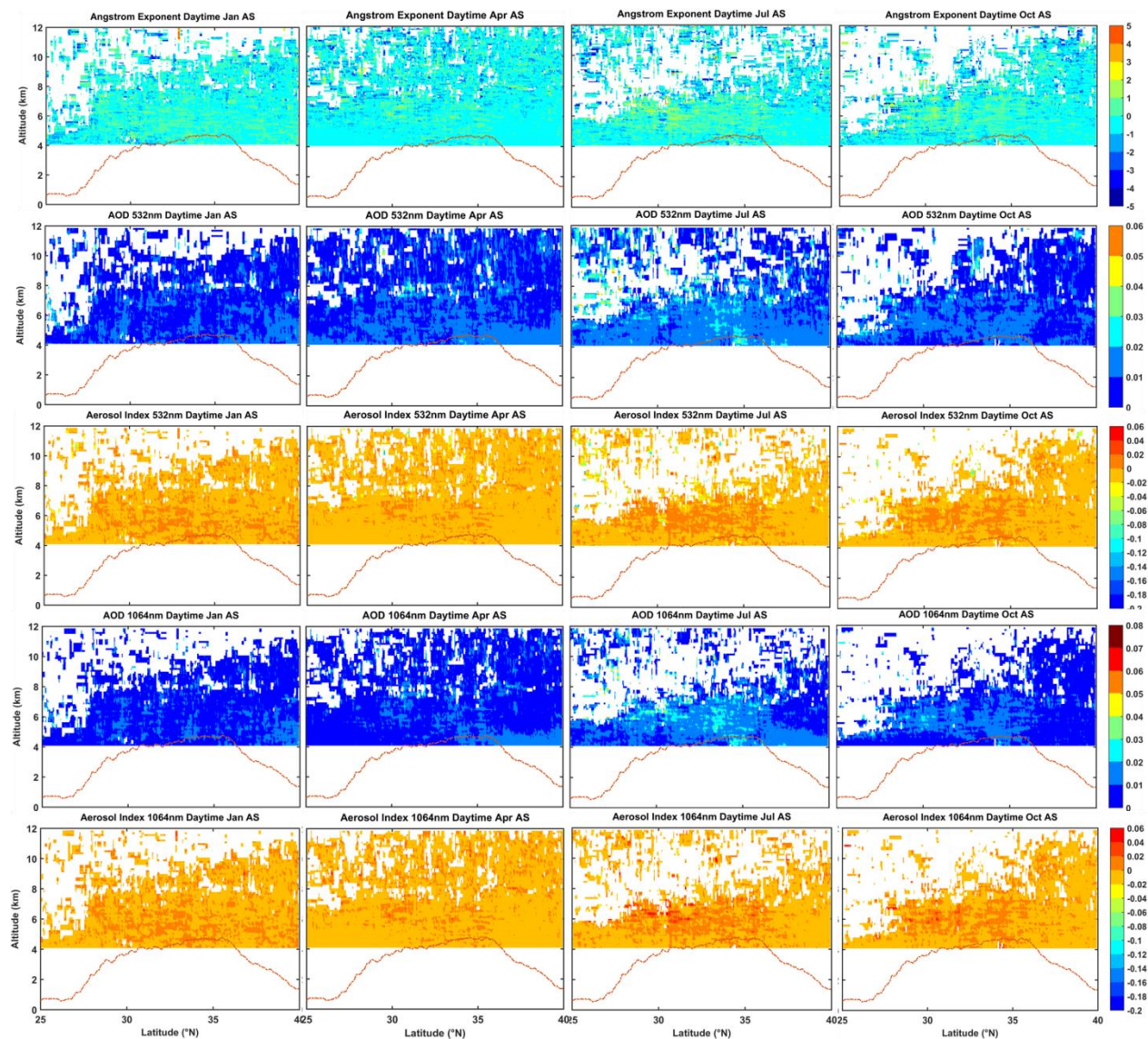
Figure 10. The monthly average construction of vertical structure of Angstrom Exponent (AE) and Aerosol Index (AI) at 532 nm and 1064 nm over Tibet Plateau (TP) for daytime during 2007-2020.

Similarly, Figure 11 includes the nighttime difference plots of aerosol EC at 532 nm between the before and after-screened for different months during 2007-2020. The difference before and after screening is immense, especially at the height of more than 5 km in the southern region of the TP in July and October. It is observed extreme outliers in the troposphere over the TP that have been recognized and eliminated. The EC detected at 1064 nm shows a similar distribution characteristic as found at 532 nm, and also includes the different attributes before and after the screened and elimination of LRAT (see Figure 12). In all seasons, AI is mainly distributed between -0.02 and 0.02. Still, the proportion between 0 and -0.02 is the largest in April and July between 4 and

490 8km. Meanwhile, AI above 8 km is mainly concentrated at 0-0.02, indicating modal

491 characteristics of vertical structure distribution of aerosol concentration and diversity

492 of aerosol types. It is worth noting that there is a large amount of aerosol over the TP in

493 January (winter), related to anthropogenic emissions of pollutants in winter and fossil

494 fuel combustion (such as black carbon and smoke). It is found that the pattern of AI is

495 more or less consistent with objective facts and phenomena.

496   Interestingly, compared with the daytime, the aerosol detected by CALIOP at night

497 can rise to a higher height and has a broader distribution range. It can be seen that

498 because the signal-to-noise ratio at night is higher than that in the daytime. The CALIOP

499 can detect smaller particles, which is also why the quality and effectiveness of CALIOP

500 night detection data are better than that in the day. After a series of correction algorithms

501 and calculating relevant parameters, we constructed the tropospheric AI climatology

502 dataset over the TP for 2007-2020.

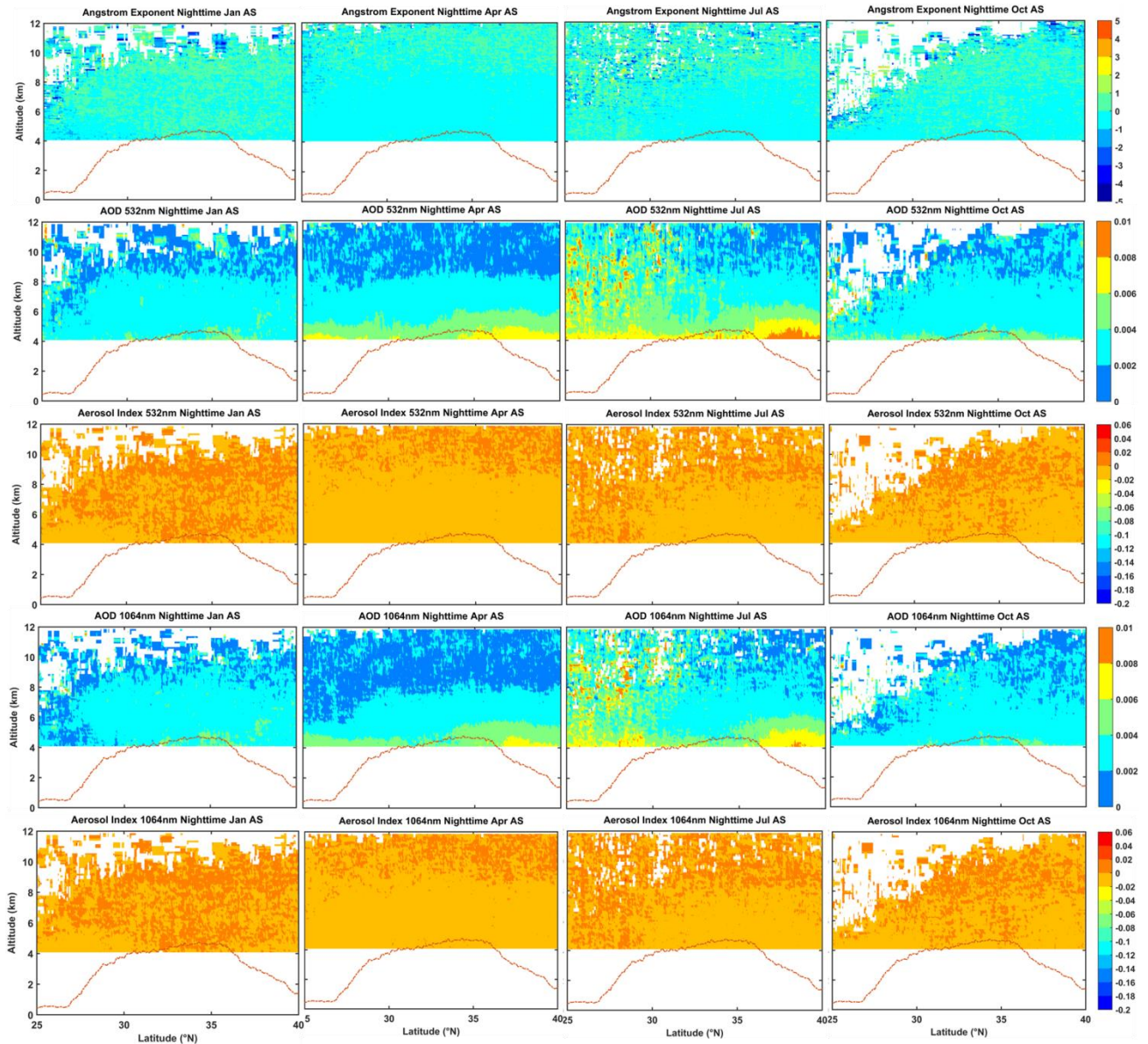504 Figure 11. The same as in Figure 8, but for nighttime at 532 nm.

23
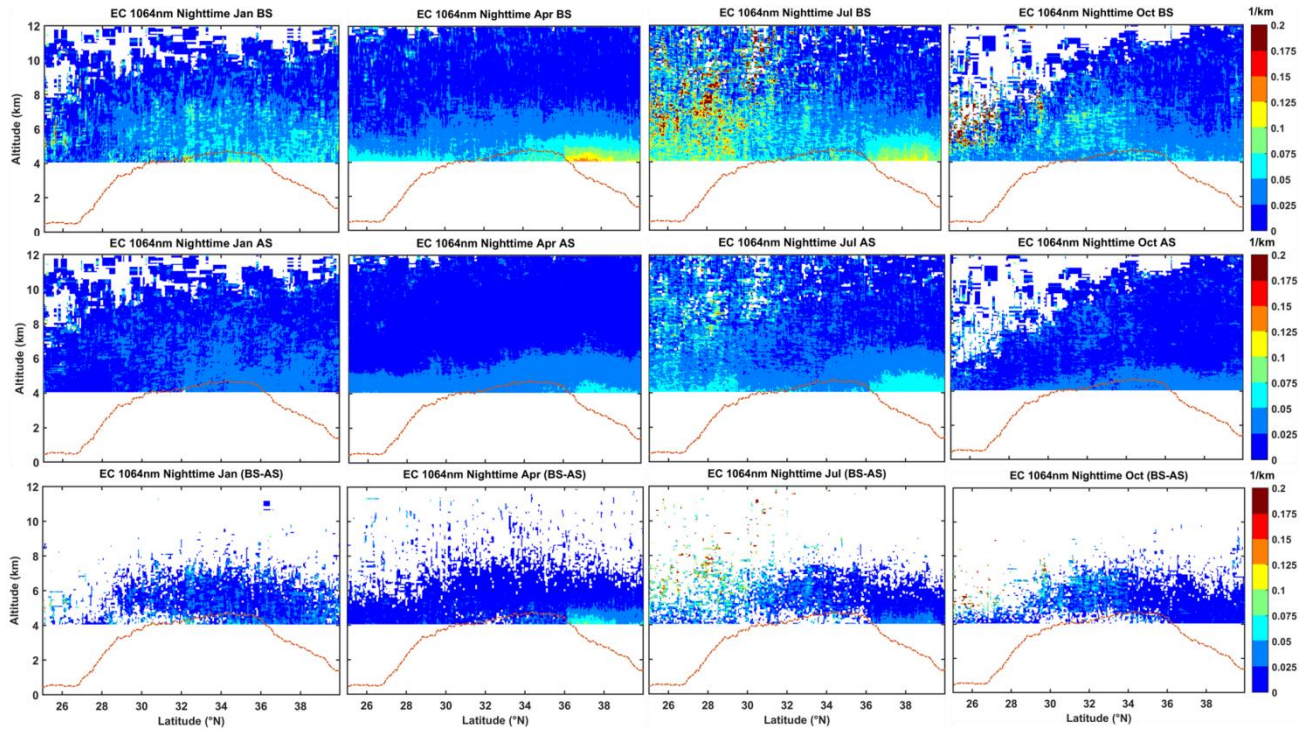
505

506 Figure 12. The same as in Figure 11, but for nighttime at 1064 nm.

507

508

509

510

Figure 13. The same as in Figure 10, but for nighttime.

3.3 Validation of the aerosol index (AI) dataset

3.3.1 Comparisons with satellite Aqua-MODIS AI products

The multiyear monthly average spatial distributions of the AE and AOD from MODIS have been shown in Figure 14, and AI was also calculated (Figure 14). The distribution of AE values over the TP in all seasons shows a decreasing trend from southeast to northwest, indicating that the particles in the upper air of the southeast region are dominated by small particles. In contrast, the particles in the upper air of the northwest region are dominated by large particles, especially in April of spring, which is related to the uplift and transmission of dust aerosol from the Taklimakan Desert to

25

the northern part of the TP in spring. Also, we can see that the AE value of Taklimakan Desert in the north of the TP in April and July in spring and summer is smaller (as the source of the sand area, mainly dust aerosol), which is smaller than in January and October in autumn and winter. AOD and AE showed opposite seasonal variation distribution patterns. According to the spatial distribution pattern of AI calculated from MODIS detection results (AE and AOD), it can be seen that the AI value over the TP is mainly between 0 and 0.4.

Figure 14 also compares the normalized frequency distribution of AI over the TP exhibiting a significant difference in all seasons from MODIS and CALIOP between before and after screening. It is evident that, in general, compared with the data results without any processing, after the elimination of the low-reliability aerosol target, the average AI value of CALIOP is closer to the result of MODIS, and the normalized frequency distribution pattern is closer to the same. Interestingly, the AI mean value and normalized frequency distribution pattern of CALIOP in April (spring) after removing the LRAT are more agreement and matched with the results of MODIS; In addition, the mean AI and normalized frequency distribution pattern of CALIOP in July (summer), and October (autumn) is more consistent with the MODIS results, and both have apparent improvement. The difference between the mean AI from CALIOP in January (winter) and the result of MODIS is relatively more extensive, but the normalized frequency distribution pattern is more consistent. This may be related to the type and chemical composition of aerosol particles that rise over the TP in different seasons and the atmospheric climate conditions unique to the topography of the TP. In brief, the accuracy of aerosol parameters AI calculated after obtaining aerosol EC with higher reliability has been dramatically improved (more or less), so even though not completely accurate, this strategy is expected to reduce the inaccuracy of the computed AI at least.

Meanwhile, it is proved that using extreme outliers as a limit to get more reliable aerosol detection information is effective and reliable. It is important to note that the 550 nm wavelength range of MODIS belongs to the visible light range, and the data products provided at the satellite transit time are the daytime detection results.

552   Therefore, here we compare and verify the daytime detection results of CALIOP (532

553   nm) with MODIS results, which are consistent in time, close in detection wavelength,

554   comparable, and representative. In addition, the quality of CALIOP daytime detection

555   data is inferior to that at night, and the reliability and accuracy of the optimized data

556   are more effectively verified by comparison with the results of MODIS. Passive

557   techniques (i.e., MODIS) have the advantage of providing a 2-D distribution of AI over

558   a wide swath, during active strategies (i.e., CALIOP) with the vertical structure of AI.

559   They are complementary and have their advantages.

560

561

562

563

564

565
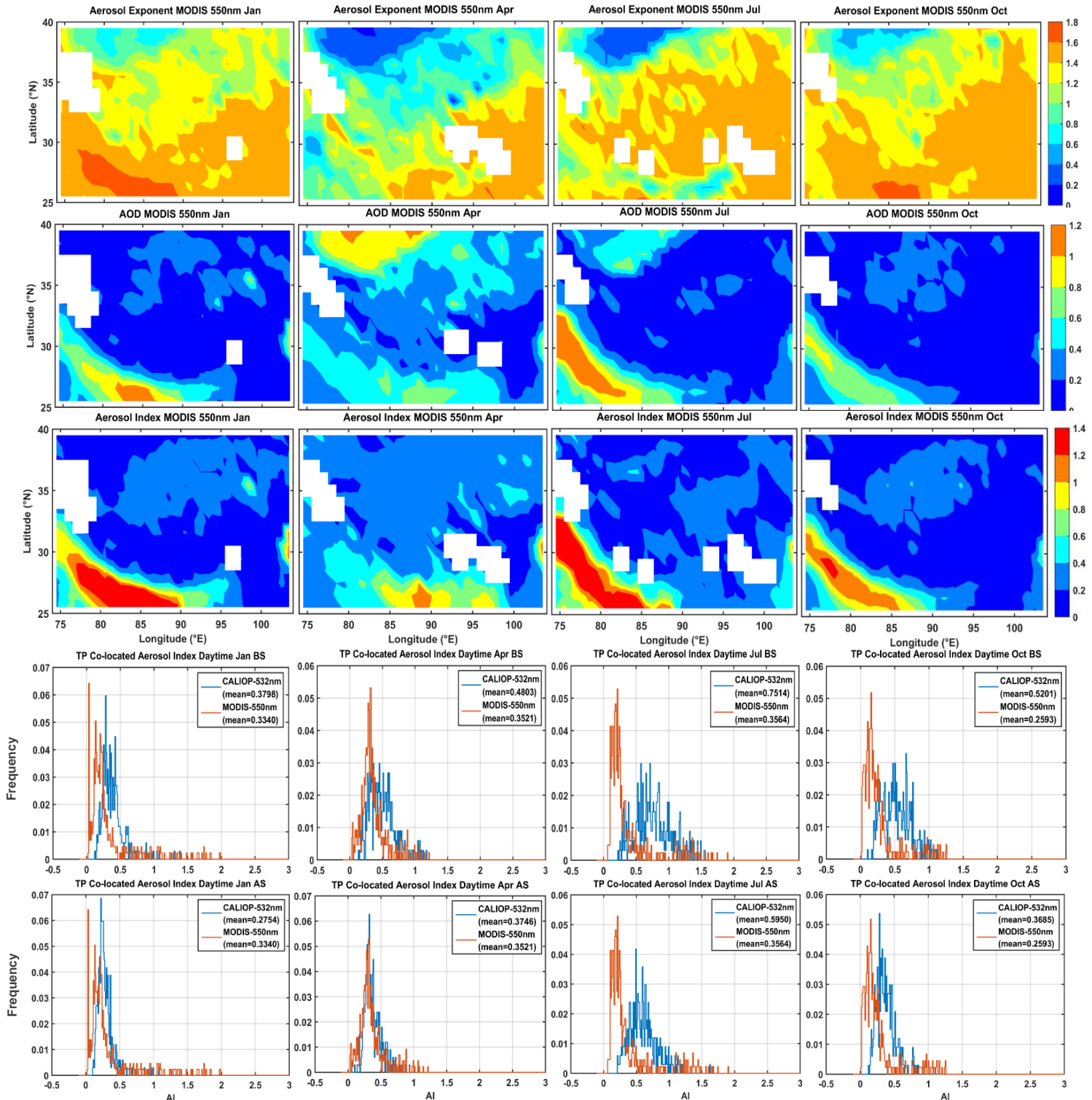
566

567

568

569

570

571

572

573

574

575

576

577

578

Figure 14. Frequency test of AI calculated by MODIS-based aerosol AE and AOD over the Qinghai Tibet Plateau and AI calculated by CALIPSO-based aerosol AE and AOD with high reliability for daytime (BS: Before Screened, the fourth line; AS: After Screened, the fifth line).

3.3.2 Performance evaluation based on in-situ Lidar observations

To further verify the performance of the AI product derived from CALIOP over

584   the TP, we chose the ground-based LIDAR observation results in the centre of the

585   Taklimakan Desert in the north of the TP to evaluate the effectiveness and accuracy of

586   the AI vertical structure of CALIOP.

587   To match the transit time of ground-based LIDAR observation and satellite

588   CALIOP observation, we extracted the EC (532 nm and 1064 nm) of ground-based

589   LIDAR during the daytime and nighttime to match the CALIOP adjacent observation

590   period, as shown in Figure 15 (observation case in TD on July 11, 2021, daytime: 03:00-

591   05:00, night: 14:00-16:00, China Beijing time, UTC+8). Considering the daytime

592   detection results of CALIOP for comparison and verification with MODIS in the above,

593   to further strengthen the inspection of CALIOP optimization results, we still choose the

594   daytime results of ground-based LIDAR detection for comparison and verification.

595   From Figure 15, it can also be seen that there are clouds or other LRAT in the daytime

596   high altitude in the ground-based LIDAR detection signal. This will be more beneficial

597   for us to check the validity and reliability of the results of the elimination of LRAT and

598   the calculated AI value.

599   Similarly, for ground-based LIDAR detection, we first reverse EC and use the IQR

600   method (see sec.2.2) to obtain extreme outliers and identify and eliminate the LRAT

601   (Figure 15). We can see that the LRAT (such as clouds and surface clutter etc.) are

602   effectively eliminated after the data optimization of 532 nm and 1064 nm detection

603   results EC. It is once again proved that it is effective and reliable to use extreme outliers

604   as a limit to obtain more reliable aerosol detection information.

605

606

607

608
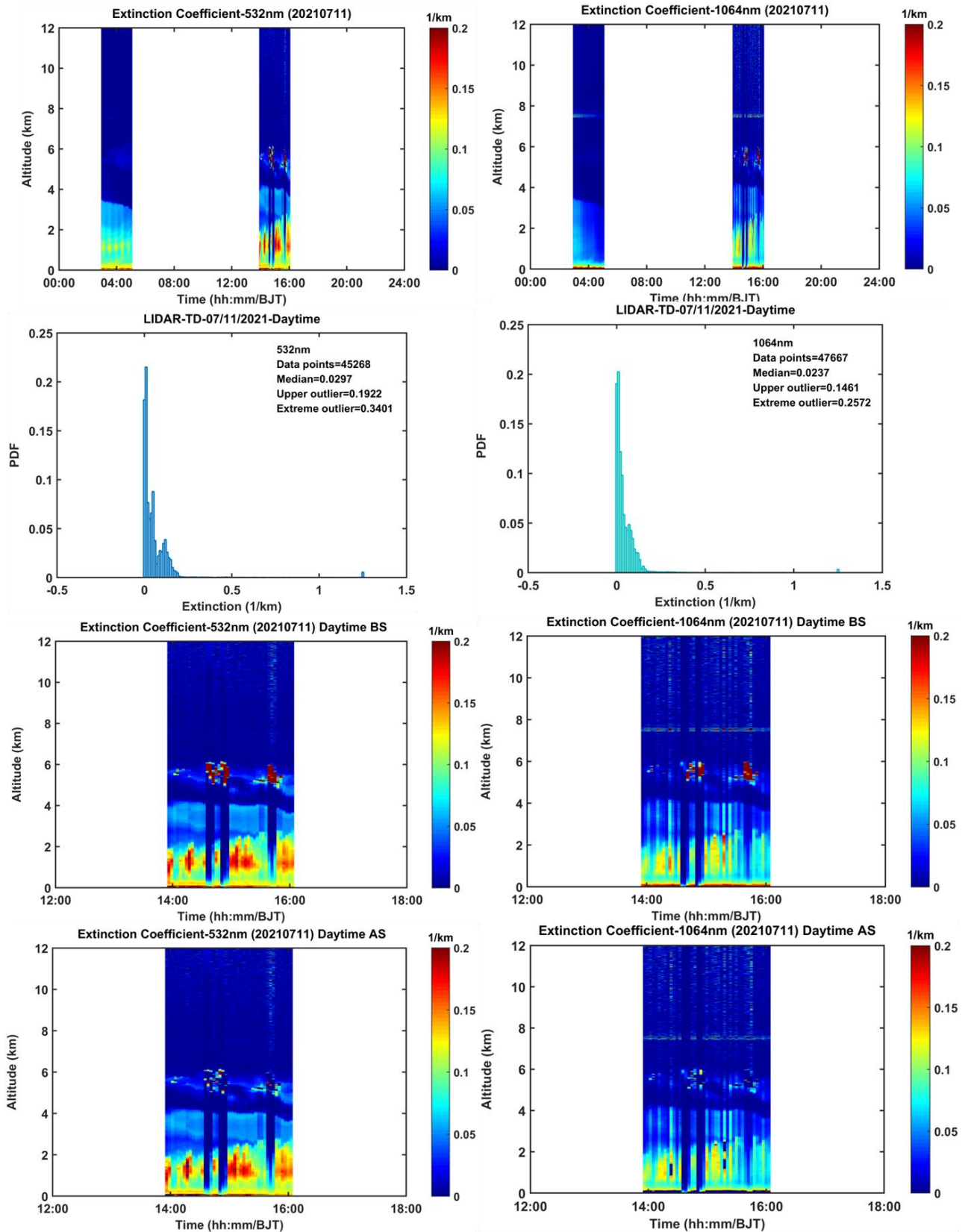
Figure 15. Elimination of low-reliability aerosol target signals detected by ground-based LIDAR in the hinterland of Taklimakan Desert.

It needs to be pointed out that the case of ground-based LIDAR detection on July

11, 2021, is quite typical, but there is a significant deviation in satellite transit, and this process cannot be well captured. To maximize and better match this process, we take the ground-based LIDAR observation in the hinterland of the Taklimakan Desert as the centre (38.967 ° N, 83.65 ° E, 1099.3m), select 38.5-39.5 ° N and 83-84 ° E range, extract the ECs observed by CALIOP transit in this range during the daytime from 2007 to July 2020, and eliminate the LRAT. After averaging the optimized data, further, calculate the AE value (as shown in Figure 16). Figure 16 depicts the detection results of ground-based LIDAR and CALIOP optimal crossing points and the comparison of calculated AI values. The AE values detected by ground-based LIDAR and CALIOP are mainly distributed between - 1 and 1, and the proportion between - 1 and 0 is the largest. The aerosol can be raised to the height of 6 km, and the higher concentration of aerosol is mainly concentrated below 2 km from the AOD vertical layer, showing a decreasing trend with the increase of height; AI values are primarily distributed between -0.02 and 0.02, and the average value and standard deviation trend of AI change with height are also basically consistent. Generally, all those facts demonstrate the agreement of the AI dataset with the CALIOP and ground-based LIDAR. Besides, all the evidence shows that after removing the LRAT, the optimized data can obtain aerosol characteristics with higher reliability.

Based on the monthly climatology AI product, we explored the average vertical structure characteristics of AI over TP during 2007-2020 (as shown in Figure 17). AI values in the daytime and at night over the TP mainly fluctuate around 0, and the standard deviation increases with the increase in altitude. The trend of AI changes with altitude is relatively consistent, and the standard deviation below 6 km is slight, indicating that the dispersion of aerosol particles is small. However, the fluctuation in the daytime is greater than that at night (the data quality at night is better than that in the daytime). In general, the detection results of 532 nm and 1064 nm can achieve complementary observation.

In general, the quality and robustness of the aerosol parameter product have improved for EC and AI with some issues that persist in the data set which we mention below:

As we do not have ground-based LIDAR detection data on the TP, we have selected ground-based LIDAR data from the centre of the Taklamakan Desert for verification and evaluation. The objectives of the verification and evaluation include the removal of low-reliability aerosol targets and the validation of the effectiveness and rationality of the constructed aerosol AI parameter results. Due to the limited detection data of ground-based LIDAR, we chose a typical aerosol process detected by ground-based LIDAR (July 11, 2021), but it did not match well with the transit time and scanning area of the CALIPSO satellite, resulting in significant errors. Therefore, we choose to compare and verify the results of the average values of July in all years within the central area of the transit Taklamakan Desert detected by CALIPSO (see the green box on the left in Figure 2). Minimize spatial errors caused by significant differences in spatial positions. This kind of error is inevitable in our data processing process and will affect the consistency of detection results to some extent.

Besides, although the monthly AI correction significantly improves the comparison between CALIPSO and MODIS, we note somewhat a larger deviation may occur in winter, and the effect after correction in summer is the best and significant, which may be related to the increased probability of mistaking clouds as aerosol particles due to more convective activities in summer. This helps us to refine our research on summer aerosols over the TP.

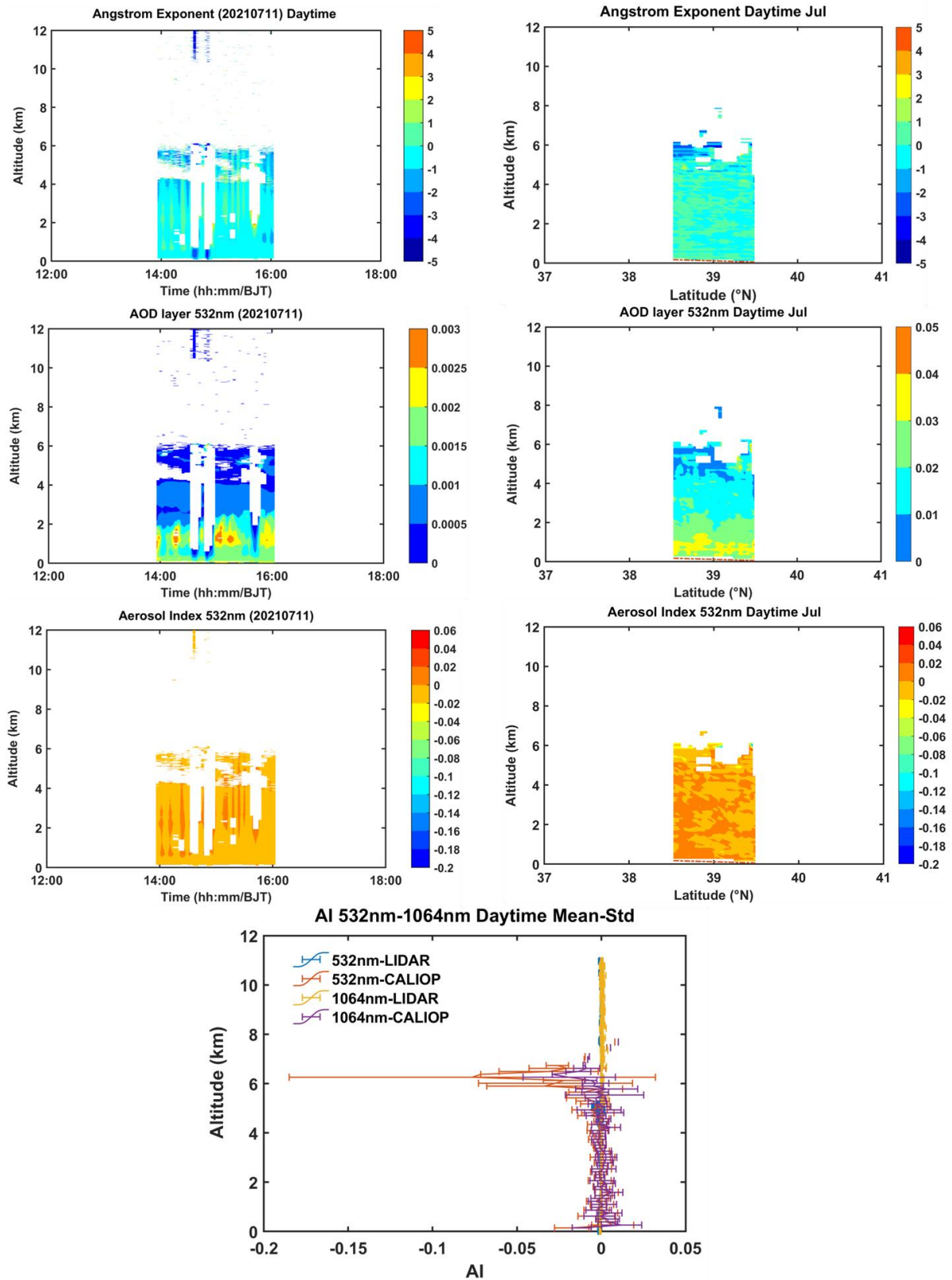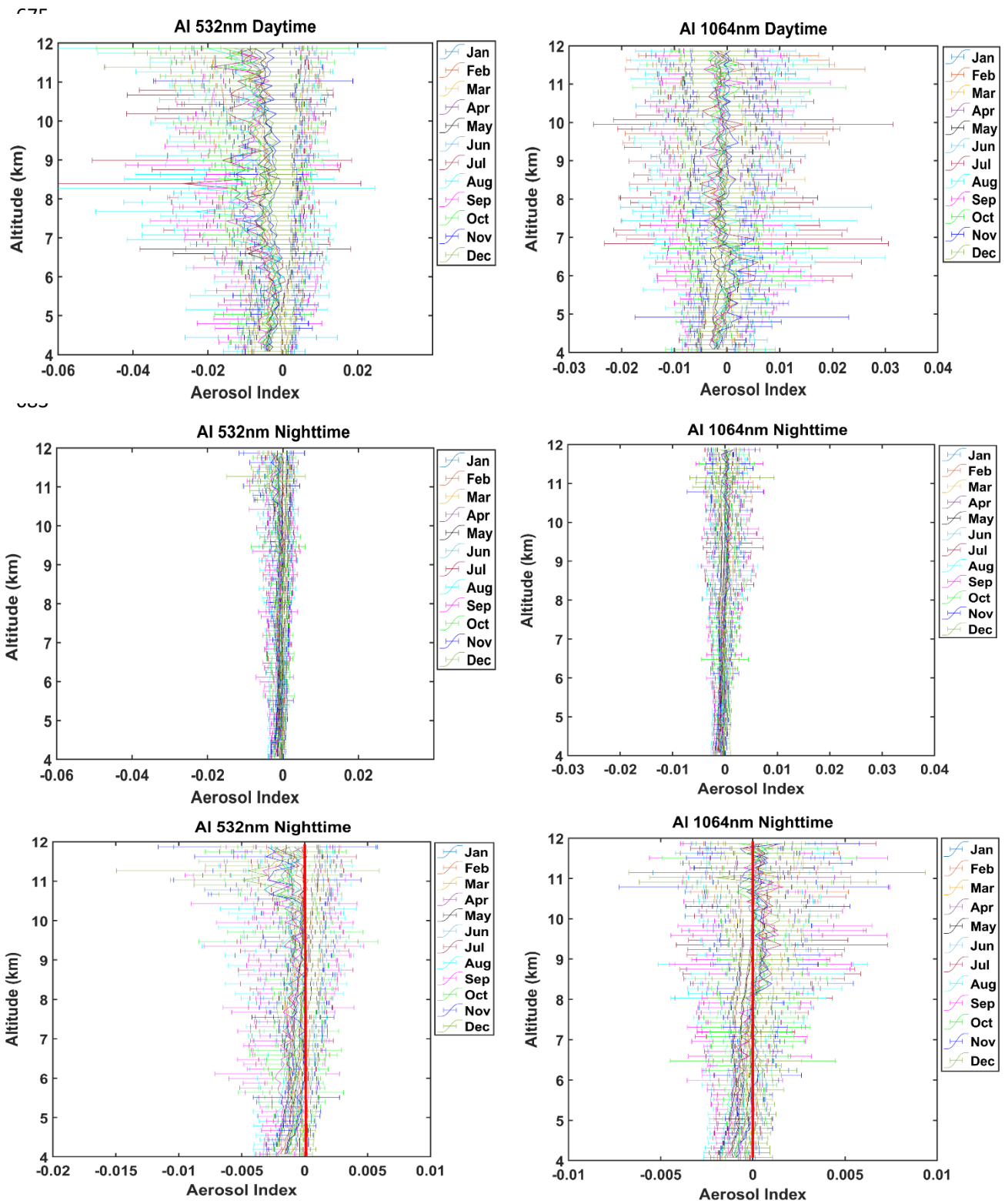Figure 16. Comparative verification of AI of CALIPSO and ground-based LIDAR remote sensing over the Taklimakan Desert region.

Figure 17. Monthly mean changes of vertical structure characteristics of AI (mean & standard deviation) over TP during 2007-2020.

4 Data availability

5 Summary and outlook

This present study is the first to report long-term, advanced-performance, high-resolution, continuous and high-quality, monthly climatology aerosol AI vertical structure from the CALIOP observation over the TP used to better understand aerosol radiation forcing under the background of accelerated climate change. Using the relationship developed when EC measurements are available, we screened the entire EC record. We assembled a climatology of high-altitude aerosol characteristics for daytime and nighttime from 2007 to 2020. In addition to providing a monthly climatology AI data set for MODIS and ground-based LIDAR validation, our data set also reveals the patterns and numbers of high-altitude vertical structure characteristics of the aerosol troposphere over the TP.

To produce accurate and higher reliability of AI values, we applied several correction procedures and rigorously checked for data quality constraints during the long observation period spanning almost 14 years (2007-2020). Nevertheless, some uncertainties remain mainly due to technical constraints, as well as limited documentation of the measurements. Even though not completely accurate, this strategy is expected to at least reduce the inaccuracy of the computed characteristic value of aerosol optical parameters. Following this initial work, we obtained vertical AI value with higher reliability. This provides information about the vertical structures of aerosol that could be used in climate models. The collection of more reliable and robust research data sets of aerosol characteristics in these extreme environments is the key basis for promoting comprehensive research on the energy balance of ground-atmosphere radiation over the Tibetan Plateau and even the global region. We expect that this data set will help some current and future research to simulate the climate change of the monthly climatology. It will also help to update future data sets and study the interaction

735 of aerosol-cloud-precipitation, thus providing sufficient observation facts and basis.

736   Finally, it should be pointed out that the AI obtained in the ultraviolet channel can

737 currently characterize both absorption and non-absorption aerosols. The AI obtained

738 from our research work cannot effectively characterize the absorption and non-

739 absorption of its aerosols, as the results we obtained are in the non-ultraviolet band

740 range, which is also an area that we need to further explore in the future. However, the

741 aerosol concentration represented by the vertical structure AI we obtained is not

742 possessed by column AOD. The significance of our work is that the AI with higher

743 reliability obtained here can more effectively obtain aerosol concentration information

744 and also presents a diversity of aerosol types at the vertical height over TP. This is the

745 main highlight of our research work. The reason why we use AI to test the results of

746 MODIS and ground LIDAR is to verify the effectiveness and reliability of AI.

747 Fortunately, the test results are very consistent and reasonable. Therefore, the AI of

748 physical meaning here can effectively characterize aerosol concentration information

749 at vertical heights.

750 **Author contributions.** HP led the reprocessing of the CALIOP, LIDAR, and

751 MODIS measurements, data analysis and the preparation of the figures, with JH and JL

752 both contributing to the design of the paper and progression of figures and text of the

753 article. ZH, MW and TZ made the original LIDAR measurements. ZH, AM and WH

754 provided the dataset and advice on the re-processing of the LIDAR and CALIOP. KRK

755 and FY contributed to either advising/co-ordinating the data recovery. All co-authors

756 performed writing sections of the paper, and/or reviewing drafts of the paper.

757

database in the present work.

References

Bucci, S., Cagnazzo, C., Cairo, F., Liberto, L.D., Fierli, F.: Aerosol variability and atmospheric transport in the Himalayan region from CALIOP 2007–2010 observations, Atmospheric Chemistry and Physics, 14(9): 4369-4381, 2014.

Boos, W., Kuang, Z.: Dominant control of the South Asian monsoon by orographic insulation versus plateau heating, Nature, 436, 218-222, 2010.

Buchard, V., Da Silva, A. M., Colarco, P. R., Darmenov, A., Randles, C. A., Govindaraju, R., Torres, O., Campbell, J., Spurr, R.: Using the OMI aerosol index and absorption aerosol optical depth to evaluate the NASA MERRA Aerosol Reanalysis, Atmospheric Chemistry and Physics, 15(10), 5743-5760, 2015.

Chen, X., Zuo, H., Zhang, Z., Cao, X., Duan, J., Zhu, C., Zhang, Z., Wang, J.: Full-coverage 250 m monthly aerosol optical depth dataset (2000–2019) amended with environmental covariates by an ensemble machine learning model over arid and semi-arid areas, NW China, Earth System Science Data, 14(12), 5233-5252, 2022.

Chen, S., Huang, J., Zhao, C., Qian, Y., Leung, L. R., Yang, B.: Modeling the transport and radiative forcing of Taklimakan dust over the Tibetan Plateau: A case study in the summer of 2006, Journal of Geophysical Research: Atmospheres, 118(2), 797-812,2013.

Chen, S., Zhang, R., Mao, R., Zhang, Y., Chen, Y., Ji, Z., Gong, Y., Guan, Y.: Sources, characteristics and climate impact of light-absorbing aerosols over the Tibetan Plateau, Earth-Science Reviews, 232, 104111,2022.

Carrió, G. G., van Den Heever, S. C., Cotton, W. R.: Impacts of nucleating aerosol on anvil-cirrus clouds: A modeling study, Atmospheric research, 84(2), 111-131, 2007.

Guan, H., Esswein, R., Lopez, J., Bergstrom, R., Warnock, A., Follette-Cook, M., Iraci, L. T.: A multi-decadal history of biomass burning plume heights identified using aerosol index measurements, Atmospheric Chemistry and Physics, 10(14), 6461-6469, 2010.

Guan, H., Chatfield, R. B., Freitas, S. R., Bergstrom, R. W., Longo, K. M.: Modeling the effect of plume-rise on the transport of carbon monoxide over Africa with NCAR CAM, Atmos. Chem. Phys., 8, 6801–6812, doi:10.5194/acp-8-6801-2008, 2008.

Goldberg, D. L., Gupta, P., Wang, K., Jena, C., Zhang, Y., Lu, Z., Streets, D. G.: Using gap-filled MAIAC AOD and WRF-Chem to estimate daily PM2:5 concentrations at 1 km resolution in the Eastern United States, Atmos. Environ., 199, 443–452, https://doi.org/10.1016/j.atmosenv.2018.11.049, 2019.

Giles, D. M., Sinyuk, A., Sorokin, M. G., Schafer, J. S., Smirnov, A., Slutsker, I., Eck, T. F., Holben, B. N., Lewis, J. R., Campbell, J. R., Welton, E. J., Korkin, S. V., and Lyapustin, A. I.: Advancements in the Aerosol Robotic Network (AERONET) Version 3 database – automated near-real-time quality control algorithm with improved cloud screening for Sun photometer aerosol optical depth (AOD) measurements, Atmos. Meas. Tech., 12, 169–209, https://doi.org/10.5194/amt-12-169-2019, 2019.

Guan, H., Esswein, R., Lopez, J., Bergstrom, R., Warnock, A., Follette-Cook, M., Fromm, M., Iraci, L. T.: A multi-decadal history of biomass burning plume heights identified using aerosol index measurements, Atmospheric Chemistry and Physics, 10(14), 6461-6469, 2010.

Hsu, N. C., Si-Chee, T., King, M. D., Herman, J. R.: Aerosol properties over bright-reflecting source regions, IEEE Trans. Geosci. Rem. Sens., 42, 557–569, 2004.

Hammer, M. S., Martin, R. V., Li, C., Torres, O., Manning, M., Boys, B. L.: Insight into global trends in aerosol composition from 2005 to 2015 inferred from the OMI Ultraviolet Aerosol Index, Atmospheric Chemistry and Physics, 18(11), 8097-8112, 2018.

Hu, Q., Wang, H., Goloub, P., Li, Z., Veselovskii, I., Podvin, T.,Li, K., Korenskiy, M.: The characterization of Taklamakan dust properties using a multiwavelength Raman polarization lidar in Kashi, China, Atmospheric Chemistry and Physics, 20(22), 13817-13834, 2020.

Hu, Y.,S.Rodier,K.Xu,W.Sun,J.Huang,B.Lin,P.Zhai,and D.Josset.: Occurrence,liquid water content, and fraction of supercooled water clouds from combined CALIOP/IIR/MODIS measurements, J.Geophys.Res., 115, D00H34, doi:10.1029/2009JD012384, 2010.

Huang, L., Jiang, J. H., Tackett, J. L., Su, H., Fu, R.: Seasonal and diurnal variations of aerosol extinction profile and type distribution from CALIPSO 5-year observations, Journal of Geophysical Research: Atmospheres, 118(10), 4572-4596, 2013.

Huang, J., Minnis, P., Chen, B., Huang, Z., Liu, Z., Zhao, Q., Yi, Y., Ayers, J. K.: Long-range transport and vertical structure of Asian dust from CALIPSO and surface measurements during PACDEX, Journal of Geophysical Research: Atmospheres, 113(D23), 2008.

Immerzeel, W., Van Beek, L., Bierkens, M.: Climate change will affect the Asian water towers, Science, 328 (5984), 1382-1385, 2010.

IPCC: Climate Change 2013: The Physical Science Basis. Contribution of Working Group I to the Fifth Assessment Report of the Intergovernmental Panel on Climate Change, edited by: Stocker, T. F., Qin, D., Plattner, G.-K., Tignor, M., Allen, S. K., Boschung, J., Nauels, A., Xia, Y., Bex, V., and Midgley, P. M., Cambridge University Press, Cambridge, United Kingdom and New York, NY, USA, 1535 pp., 2013.

IPCC, 2021: Climate Change 2021: The Physical Science Basis. Contribution of Working Group I to the Sixth Assessment Report of the Intergovernmental Panel

855   on Climate Change, edited by: Masson-Delmotte, V., P. Zhai, A. Pirani, S.L.

856   Connors, C. Péan, S. Berger, N. Caud, Y. Chen, L. Goldfarb, M.I. Gomis, M.

857   Huang, K. Leitzell, E. Lonnoy, J.B.R. Matthews, T.K. Maycock, T. Waterfield, O.

858   Yelekçi, R. Yu, and B. Zhou (eds.)]. Cambridge University Press, Cambridge,

859   United Kingdom and New York, NY, USA, In press, doi:10.1017/9781009157896.

860 Iglewicz, B. and Hoaglin, D.: How to Detect and Handle Outliers, ASQC basic

861   references in quality control, ASQC Quality Press, Milwaukee, 1993.

862 Kovilakam, M., Thomason, L. W., Ernest, N., Rieger, L., Bourassa, A., Millán, L.: The

863   global space-based stratospheric aerosol climatology (version 2.0): 1979–2018,

864   Earth System Science Data, 12(4), 2607-2634, 2020.

865 Kahn, R. A., Gaitley, B. J., Garay, M. J., Diner, D. J., Eck, T. F., Smirnov, A., Holben,

866   B. N.: Multiangle Imaging SpectroRadiometer global aerosol product assessment

867   by comparison with the Aerosol Robotic Network, J. Geophys. Res.-Atmos., 115,

868   D23209, doi:10.1029/2010jd014601, 2010.

869 Kojima, T., Buseck, P. R., Wilson, J. C., Reeves, J. M., Mahoney, M. J.: Aerosol

870   particles from tropical convective systems: Cloud tops and cirrus anvils, Journal

871   of Geophysical Research: Atmospheres, 109(D12), 2004.

872 Kim, M.H., Omar, A.H., Tackett, J.L., Vaughan, M.A., Winker, D.M., Trepte, C.R., Hu,

873   Y.,Liu, Z., Poole, L.R., Pitts, M.C., Kar, J., Magill, B.E.: The CALIPSO Version 4

874   Automated Aerosol Classification and Lidar Ratio Selection Algorithm,

875   Atmospheric Measurement Techniques, 11(11):6107-6135,2018.

876 Liu, Y., Huang, J., Wang, T., Li, J., Yan, H., He, Y.: Aerosol-cloud interactions over the

877   Tibetan Plateau: An overview, Earth-Science Reviews, 104216, 2022.

878 Liu, Y., Li, Y., Huang, J., Zhu, Q., Wang, S.: Attribution of the Tibetan Plateau to

879   northern drought, National Science Review, 7(3), 489-492, 2020.

880 Liu, Y., Hua, S., Jia, R., Huang, J.: Effect of aerosols on the ice cloud properties over

881   the Tibetan Plateau, Journal of Geophysical Research: Atmospheres, 124(16),

882   9594-9608, 2019.

883 Luo, H., Yanai, M.: The large-scale circulation and heat sources over the Tibetan

884   Plateau and surrounding areas during the early summer of 1979, Part II: Heat and

moisture budgets, Mon. Wea. Rev., 112, 966–989, 1984.

Liou, K.: Influence of cirrus clouds on weather and climate processes: a global perspective, Mon. Weather Rev., 114, 1167–1199,1986.

Liu, Z., Kar, J., Zeng, S., Tackett, J., Vaughan, M., Avery, M., Pelon, J., Getzewich, B., Lee, K.P., Magill, B., Omar, A., Lucker, P., Trepte,C., Winker, D.: Discriminating between clouds and aerosols in the caliop version 4.1 data products, Atmos. Meas. Tech., 12, 703–734, 2019.

Liu, D., Z. Wang, Z. Liu, D. Winker, C. Trepte.: A height resolved global view of dust aerosols from the first year CALIPSO lidar measurements, J. Geophys. Res., 113, D16214, doi:10.1029/2007JD009776, 2008.

Liu, Z., Liu, D., Huang, J., Vaughan, M., Uno, I., Sugimoto, N., Kittaka, C., Trepte, C., Wang, Z., Hostetler, C., Winker, D.: Airborne dust distributions over the Tibetan Plateau and surrounding areas derived from the first year of CALIPSO lidar observations, Atmospheric Chemistry and Physics, 8(16), 5045-5060, 2008.

Liu, P. F., C. S. Zhao, Q. Zhang, Z. Z. Deng, M. Y. Huang, X. C. Ma, X. X. Tie.: Aircraft study of aerosol vertical distributions over Beijing and their optical properties, Tellus, Ser. B, 61(5), 756–767, doi:10.1111/j.1600-0889.2009.00440.x, 2009.

Molnar,P., Boos,W., Battisti, D.: Orographic controls on climate and paleoclimate of Asia: thermal and mechanical roles for the Tibetan Plateau, Annu. Rev. Earth Pl.Sc., 38 (1), 77-102, 2010.

Matsuki, A., Iwasaka, Y., Osada, K., Matsunaga, K., Kido, M., Inomata, Y., Trochkine, D., Nishita, C., Nezuka, T., Sakai,T., Zhang,D., Kwon, S. A.: Seasonal dependence of the long‐range transport and vertical distribution of free tropospheric aerosols over east Asia: On the basis of aircraft and lidar measurements and isentropic trajectory analysis, Journal of Geophysical Research: Atmospheres, 108(D23), 2003.

Nieberding, F., Wille, C., Fratini, G., Asmussen, M. O., Wang, Y., Ma, Y., Sachs, T.: A long-term (2005–2019) eddy covariance data set of CO2 and H2O fluxes from the Tibetan alpine steppe, Earth System Science Data, 12(4), 2705-2724, 2020.

Nakajima, T., Higurashi, A., Kawamoto, K., Penner, J. E.: A possible correlation

between satellite‐derived cloud and aerosol microphysical parameters, Geophysical Research Letters, 28 (7), 1171-1174, https://doi.org/10.1029/2000GL012186, 2001.

Pan, H., Huo, W., Wang, M., Zhang, J., Meng, L., Kumar, K. R., Devi, N. L.: Insight into the climatology of different sand-dust aerosol types over the Taklimakan Desert based on the observations from radiosonde and A-train satellites, Atmospheric Environment, 238, 117705, 2020.

Qiu, J.: China: The third pole, Nature, 454, 393-396, https://doi.org/10.1038/454393a, 2008.

Rossow, W., Schiffer, R.: Advances in understanding clouds from ISCCP, Bull. Am. Meteorol. Soc., 80, 2261‐2287, 1999.

Rieger, L. A., Bourassa, A. E., Degenstein, D. A.: Merging the OSIRIS and SAGE II stratospheric aerosol records, J. Geophys. Res. Atmos., 120, 8890–8904, https://doi.org/10.1002/2015JD023133, 2015.

Rieger, L. A., Zawada, D. J., Bourassa, A. E., Degenstein, D. A.: A Multiwavelength Retrieval Approach for Improved OSIRIS Aerosol Extinction Retrievals, J. Geophys. Res.-Atmos., 124, 7286–7307, https://doi.org/10.1029/2018JD029897, 2019.

Seifert, P., Ansmann, A., Müller, D., Wandinger, U., Althausen, D., Heymsfield, A. J., Massie, S.T., Schmitt, C.: Cirrus optical properties observed with lidar, radiosonde, and satellite over the tropical Indian Ocean during the aerosol-polluted northeast and clean maritime southwest monsoon, Journal of Geophysical Research: Atmospheres, 112(D17), 2007.

Sasano, Y.: Tropospheric aerosol extinction coefficient profiles derived from scanning lidar measurements over Tsukuba, Japan from 1990 to 1993, Appl. Opt., 35(24), 4941–4952, 1996.

Thomason, L. W. and Vernier, J.-P.: Improved SAGE II cloud/aerosol categorization and observations of the Asian tropopause aerosol layer: 1989–2005, Atmos. Chem. Phys., 13, 4605–4616, https://doi.org/10.5194/acp-13-4605-2013, 2013.

Twomey, S.A.: The influence of pollution on the shortwave albedo of clouds, J. Atmos.

Sci., 34 (7), 1149－1154,1977.

Torres, O., Bhartia, P. K., Herman, J. R., Ahmad, Z., and Gleason, J.: Derivation of aerosol properties from satellite measurements of backscattered ultraviolet radiation: Theoretical basis, J. Geophys. Res., 103, 17099–17110, doi:10.1029/98JD00900, 1998.

Torres, O., Tanskanen, A., Veihelmann, B., Ahn, C., Braak, R., Bhartia, P. K., Veefkind, P., Levelt, P.: Aerosols and surface UV products from Ozone Monitoring Instrument observations: An overview, J. Geophys. Res., 112, D24S47, doi:10.1029/2007JD008809, 2007.

Vernier, J. P., Fairlie, T. D., Natarajan, M., Wienhold, F. G., Bian, J., Martinsson, B. G., Crumeyrolle, S., Thomason, L.W., Bedka, K. M.: Increase in upper tropospheric and lower stratospheric aerosol levels and its potential connection with Asian pollution, Journal of Geophysical Research: Atmospheres, 120(4), 1608-1619, 2015.

Wan, B., Gao, Z., Chen, F., Lu, C.: Impact of Tibetan Plateau surface heating on persistent extreme precipitation events in Southeastern China, Mon. Weather Rev., 145 (9), 3485–3505, 2017.

Winker, D. M., Vaughan, M. A., Omar, A., Hu, Y., Powell, K. A., Liu, Z., Hunt, W. H., and Young, S. A.: Overview of the CALIPSO mission and CALIOP data processing algorithms, J. Atm. Ocean. Techn., 26, 2310–2323, 2009.

Winker, D.M., Hunt, W.H., McGill, M.J.: Initial performance assessment of CALIOP, Geophys. Res. Lett., 34, L19803, https://doi.org/10.1029/2007GL030135, 2007.

Wu, G., Zhang, Y.: Tibetan Plateau forcing and the timing of the monsoon onset over South Asia and the South China Sea, Mon. Wea. Rev., 126, 913-927,1998.

Wu, G., Liu, Y., Zhang, Q., Duan, A., Wang, T., Wan, R., Liu, X., Li, W., Wang, Z., Liang, X.: The influence of mechanical and thermal forcing by the Tibetan Plateau on Asian climate, J. Hydro. Meteor. Spec. Sect., 8 (4), 770-789, 2007.

Wu, G., Liu, Y., Dong, B., Liang, X., Duan, A., Bao, Q., Yu, J.: Revisiting Asian monsoon formation and change associated with Tibetan Plateau forcing: I. Formation, Climate dynamics, 39, 1169-1181, 2012.

Wu, G., Duan, A., Liu, Y., Mao, J., Ren, R., Bao, Q., He, B., Liu, B., Hu, W.: Tibetan Plateau climate dynamics: recent research progress and outlook, Natl. Sci. Rev., 2 (1), 100-116, 2015.

Wei, X., Bai, K., Chang, N.-B., Gao, W.: Multi-source hierarchical data fusion for high-resolution AOD mapping in a forest fire event, International Journal of Applied Earth Observation and Geoinformation, 102, 102366, https://doi.org/10.1016/j.jag.2021.102366, 2021.

Xu, X., Lu, C., Shi, X., Gao, S.: World water tower: an atmospheric perspective, Geophys. Res. Lett., 35 (20), 2008.

Xu, C., Ma, Y. M., You, C., Zhu, Z. K.: The regional distribution characteristics of aerosol optical depth over the Tibetan Plateau, Atmospheric Chemistry and Physics, 15(20), 12065-12078, 2015.

Yanai, M., Li, C., Song, Z.: Seasonal heating of the Tibetan Plateau and its effects on the evolution of the Asian summer monsoon, J. Meteor. Soc. Japan 70, 319-351,1992.

Zhang, S., Huang, Z., Li, M., Shen, X., Wang, Y., Dong, Q., Bi J., Zhang J., Li W., Li Z., Song, X.: Vertical structure of dust aerosols observed by a ground-based raman lidar with polarization capabilities in the center of the Taklimakan desert, Remote Sensing, 14(10), 2461, 2022.

Zhang, S., Huang, Z., Alam, K., Li, M., Dong, Q., Wang, Y., Shen, X., Bi, J., Zhang, J., Li, W., Li, Z., Wang, W., Cui, Z., Song, X.: Derived Profiles of CCN and INP Number Concentrations in the Taklimakan Desert via Combined Polarization Lidar, Sun-Photometer, and Radiosonde Observations, Remote Sensing, 1–20. https://doi.org/10.3390/rs15051216, 2023.

Zhou, J., G. Yu, C. Jin, F. Qi, D. Liu, H. Hu, Z. Gong, G. Shi, T. Nakajima, T. Takamura.: Lidar observations of Asian dust over Hefei, China in Spring 2000, J. Geophys. Res., 107(D15), 4252, doi:10.1029/,2002.2001JD000802, 2002.